Precambrian Research 262 (2015) 1–19

Contents lists available at ScienceDirect

Precambrian Research

journal homepage: www.elsevier.com/locate/precamres

Charnockites and UHT metamorphism in the Bakhuis Granulite Belt, western Suriname: Evidence for two separate UHT events

Martijn Klaver[a,*], Emond W.F. de Roever[a], Josefine A.M. Nanne[a,b], Paul R.D. Mason[c], Gareth R. Davies[a]

[a] Department of Geology and Geochemistry, VU University Amsterdam, The Netherlands
[b] Department of Earth Sciences, Durham University, United Kingdom
[c] Faculty of Geosciences, Utrecht University, The Netherlands

ARTICLE INFO

Article history:
Received 3 November 2014
Received in revised form 31 January 2015
Accepted 5 February 2015
Available online 17 February 2015

Keywords:
Charnockite
Ultrahigh-temperature metamorphism
Bakhuis Granulite Belt
Guiana Shield
Zircon geochronology

ABSTRACT

The Bakhuis Granulite Belt in western Suriname is an ultrahigh-temperature (UHT) metamorphic terrain in the centre of the Paleoproterozoic (Transamazonian) Guiana Shield. Next to the UHT granulites, the belt contains a 30 by 30 km body of orthopyroxene-bearing granitoids: the Kabalebo charnockites. This setting offers an excellent opportunity to investigate the source and origin of charnockite magmatism and the common association of charnockites with (ultra)high-temperature metamorphic terrains. We present a detailed geochemical dataset and LA-ICPMS zircon U/Pb ages with the aim to investigate the geochemical and geochronological relationship between charnockite magmatism and UHT metamorphism in the Bakhuis Granulite Belt. The Kabalebo charnockites have a characteristic trace element signature with elevated K_2O, P_2O_5, Zr, REE and Ba coupled with mobile element depletion, which is a consequence of high-temperature melting of anhydrous but fertile granulitic crust. Field and geochemical evidence suggests that the intermediate granulites in the Bakhuis Granulite Belt are the source of the Kabalebo charnockites. The new U/Pb zircon ages indicate that charnockite magmatism (1993–1984 Ma) postdates UHT metamorphism (2.07–2.05 Ga) by at least 60 Myr. We argue that it is not possible to maintain a thermal anomaly >200 °C in excess of a normal geothermal gradient for such a prolonged period and hence conclude that the Bakhuis Granulite Belt has experienced two distinct periods in which temperatures >950 °C were reached in the lower crust.

The presence of comagmatic metadolerite enclaves in the charnockites establishes that mafic magmatism occurred contemporaneously with, and was the likely heat source for, charnockite magmatism at 1.99–1.98 Ga. In contrast, the 2.07–2.05 Ga UHT metamorphic event is not associated with felsic or mafic magmatism in the Bakhuis Granulite Belt or nearby Guiana Shield and postdates the suturing of the juvenile North Guiana TTG-greenstone belt with the West African Shield by at least 10 Myr. We postulate that the UHT metamorphism at 2.07–2.05 Ga is the result of mantle upwelling in a slab tear in the subducted West African slab that formed as the result of crustal scale shearing and boudinage. Prior to the final stabilisation of the Amazonian–West African Shield at 1.90 Ga, northward subduction at 1.99–1.98 Ga caused the emplacement of voluminous hot, mafic magma, resulting in partial melting of the Bakhuis granulite suite to form the Kabalebo charnockites. Charnockite magmatism was roughly contemporaneous with the emplacement of a large belt of shallow granites and felsic volcanic rocks in the SW Guiana Shield. Despite their similar age, the inherited zircon populations suggest that the charnockites are derived from a distinct, juvenile source while the felsic volcanic rocks include an Archaean protolith.

1. Introduction

Charnockites are orthopyroxene-bearing granitoid rocks that occur in a wide variety of tectonic settings with a diversity of field relationships that suggests multiple modes of formation (Bhattacharya, 2010; Frost and Frost, 2008; Rajesh and Santosh, 2012). Magnesian, calc-alkalic charnockites form a common rock type in high-grade metamorphic terrains and are regularly

* Corresponding author at: De Boelelaan 1085, 1081HV Amsterdam, The Netherlands. Tel.: +31 020 59 83725.
E-mail address: martijn.klaver@vu.nl (M. Klaver).

http://dx.doi.org/10.1016/j.precamres.2015.02.014
0301-9268/

associated with ultrahigh-temperature (UHT) metamorphic rocks (Bhattacharya, 2010; Frost and Frost, 2008; Newton, 1992). These charnockites are often contemporaneous with peak metamorphic conditions (e.g. Korhonen et al., 2013; Peng et al., 2010), but can also be generated during subduction preceding the collisional event and UHT metamorphism (e.g. Rajesh et al., 2014) or due to post-collisional decompression (Newton, 1992; Zhao et al., 1997). The post-collisional charnockites often have a characteristic trace element signature of high K_2O, TiO_2, P_2O_5 and Zr combined with low fluid-mobile element (Cs–Rb–U–Th) concentrations, which is obtained through melting of dehydrated but fertile lower crust at elevated crustal temperatures (e.g. Kilpatrick and Ellis, 1992; Young et al., 1997; Zhao et al., 1997). Regardless whether charnockites are pre-, syn- or post-collisional, crustal melting at temperatures >900 °C and UHT metamorphism generally require an external heat source (Brown and Korhonen, 2009; Clark et al., 2011; Collins, 2002). Primitive mantle melts play a potentially important role in facilitating UHT conditions, even though voluminous (ultra)mafic rocks are scarce in many UHT occurrences (Kelsey and Hand, 2014). Nevertheless, mafic underplating has been proposed as the heat source (e.g. Liu et al., 2006), but recently ridge subduction has been inferred as the dominant process responsible for charnockite magmatism and ultrahigh-temperature (UHT) metamorphism in several locations (e.g. Peng et al., 2012; Santosh et al., 2012; Zhang et al., 2010).

A 30 by 30 km body of igneous charnockite, the Kabalebo charnockites, has been recognised in the southwest of the Bakhuis Granulite Belt (BGB) in western Suriname. The BGB is located in the centre of the Paleoproterozoic Guiana Shield and experienced UHT metamorphism (max. 1000–1050 °C at 0.85 GPa) at the end of the main phase of the Transamazonian Orogeny at 2.07–2.05 Ga (De Roever et al., 2003; Delor et al., 2003a). Emplacement of the Kabalebo charnockites was believed to be contemporaneous with the UHT event (De Roever et al., 2003; Kroonenberg and de Roever, 2010), similar to the charnockite magmatism and UHT metamorphism documented in the North China Craton by Peng et al. (2010) or Limpopo Mobile Belt by Rajesh et al. (2014). Geochronological confirmation, however, is lacking. Here we report a detailed petrogenetic study of the Kabalebo charnockites and granulites, including LA-ICPMS zircon U–Pb dating, to investigate the association of charnockite magmatism and UHT metamorphism in the BGB. To aid the interpretation of the new geochronological data, a major-, trace elements and Sr–Nd isotope study of the Kabalebo charnockites complemented with trace element and Hf isotope analysis on the dated zircons was performed. The new data are used to refine the current models for the evolution of the Guiana Shield during the Transamazonian Orogeny.

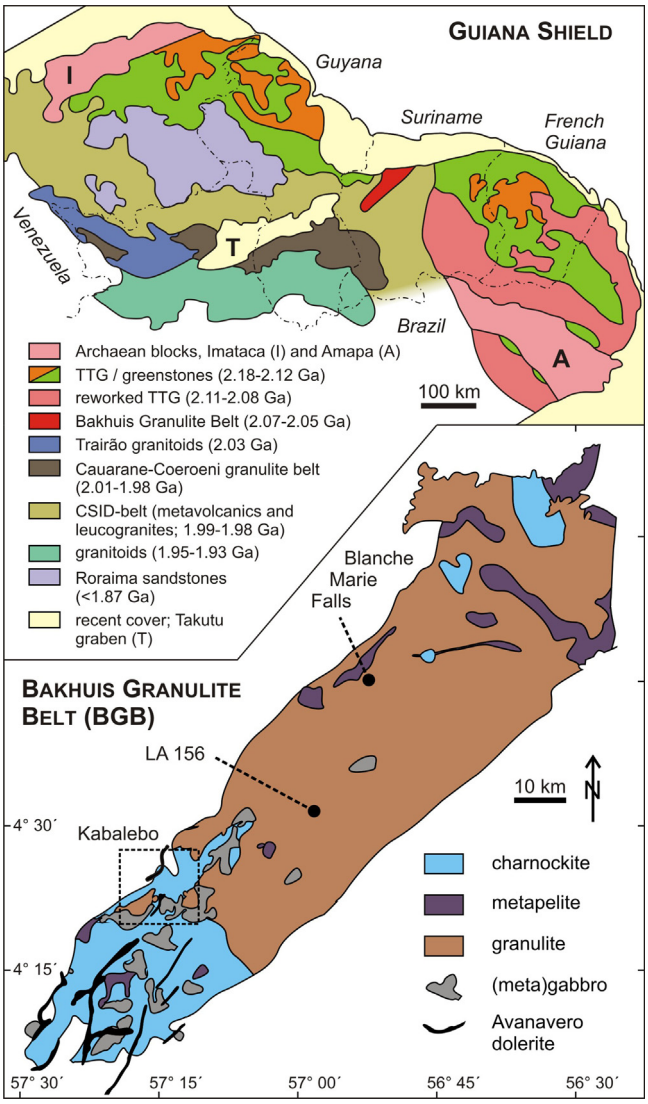

Fig. 1. Geological map of the Transamazonian Guiana Shield and Bakhuis Granulite Belt, modified after Delor et al. (2003a), Fraga et al. (2009) and De Roever et al. (2003). The lower map of the BGB is a detailed map of the red region in the upper Guiana Shield map. The dashed box labelled "Kabalebo" in the BGB map indicates the sampling area of the Kabalebo charnockites. See text for further discussion.

2. Geological setting

The Bakhuis Mountains in western Suriname are the topographical expression of a high-grade metamorphic belt: the Bakhuis Granulite Belt (BGB; Fig. 1). The NE–SW oriented belt, approximately 30–40 km wide and 100 km long, is incorporated in a horst-like structure bounded on both sides by steeply dipping shear zones. Rubidium–strontium and K–Ar ages determined on micas indicate formation of these shear zones during the Nickerie metamorphic event at 1.2 Ga (Cordani et al., 2010; Priem et al., 1971). Metapelitic lenses, banding and foliation in the belt reflect an elongated dome structure, which is cut off by the SE shear zone. Doming and exhumation might have initiated at the end of the main phase of the Transamazonian Orogeny (~2.06 Ga) and subsequent reactivation during the Tertiary gave the belt its present-day shape (Delor et al., 2003a).

The granulite suite of the BGB consists of mafic (30–35%) and intermediate (55%) granulites. Metapelites and quartzitic lithologies constitute the remaining 10–15% of the suite. Conspicuous and common compositional banding at the centimeter to meter scale and the presence of intercalated metapelitic, spessartine quartzite and calc-silicate bands suggest a predominantly sedimentary and/or volcanic protolith of the granulites. Orthopyroxene is invariably present in the granulite suite and its occurrence as a primary phase in leucosomes indicates migmatisation under granulite facies conditions. Peak metamorphic conditions reached 950–1050 °C at 0.85–0.90 GPa and hence the BGB is classified as an ultrahigh-temperature metamorphic terrain (De Roever et al., 2003). In the southwest of the belt, the granulites show an abrupt transition to orthopyroxene-bearing granitoids: the Kabalebo charnockites. Gabbroic and metagabbroic intrusions are scattered throughout the belt but occur more frequently in the southwest. Narrow metadolerite dikes are a common feature in the BGB. A variable degree of metamorphic overprint of the mafic bodies and dikes suggests that multiple generations of

mafic intrusives are present, but geochronological confirmation is so far absent.

Tectonically, the BGB is located in the centre of the Paleoproterozoic Guiana Shield (Fig. 1). Apart from the Archaean Imataca and Amapa blocks in the western and eastern edges of the shield, the Guiana Shield formed during the Transamazonian Orogeny (2.26–1.95 Ga) as a result of the collision between the West African Shield and Amazonian Craton (Delor et al., 2003a). The 2.18–2.12 Ga North Guiana tonalite–trondhjemite–granodiorite (TTG) greenstone belt constitutes the northern margin of the shield and was formed as the result of southward subduction of oceanic crust. Suturing of the TTG-greenstone belt with the West African Shield occurred at 2.11–2.08 Ga (Delor et al., 2003a; Hildebrand et al., 2014; Norcross et al., 2000; Padoan et al., 2014) and was rapidly followed by the collision with the Archaean Amapa terrain in the east (da Rosa-Costa et al., 2006, 2008; Delor et al., 2003b). Ultrahigh-temperature metamorphism in the BGB at 2072–2055 Ma (De Roever et al., 2003) postdates these collisional events and marks the end of the main phase of the Transamazonian Orogeny. The BGB is surrounded to the W, S and E by subvolcanic granites and metavolcanic rocks of the Cuchivero–Surumu–Iwokrama–Dalbana (CSID) belt that intruded the Guiana Shield during the late-Transamazonian phase at 1.99–1.98 Ga (De Roever et al., 2010; Delor et al., 2003a; Nadeau et al., 2013; Reis et al., 2000). The subvolcanic granites and metavolcanic rocks of the CSID-belt were subsequently intruded by biotite granite in W Suriname, which is probably equivalent to the ~1.97–1.95 Ga I- and S-type granitoids in Roraima, Brazil (Almeida et al., 2007; Reis et al., 2000). To the south of the CSID-belt lies the Cauarane-Coeroeni granulite belt (CCB), which is clearly distinct from the BGB by a lower metamorphic grade (peak PT ~800 °C; Kroonenberg, 1976). Two distinct metamorphic events are recognised in the CCB, the oldest of which is dated at 2.01–1.98 Ga and the younger phase at 1.97–1.96 Ga (De Roever et al., 2010; Fraga et al., 2009; Nadeau et al., 2013). Extensive post-collisional <1.90 Ga granitoid magmatism is present to the southwest of the CCB in Guyana and Brazil (Kroonenberg and de Roever, 2010; Santos et al., 2004; Valério et al., 2009). After the Transamazonian Orogeny, three generations of mafic dike swarms intruded the Guiana Shield, all of which are present in the BGB.

3. Analytical techniques

Full analytical details are given in the online supplementary material and only the most pertinent information is provided here. Major element concentrations were measured by X-ray fluorescence spectroscopy (XRF) and trace elements by inductively coupled plasma mass spectrometry (ICP-MS). Strontium and neodymium isotopes were measured by thermal ionisation mass spectrometry (TIMS). Results for reference materials are listed in the online supplementary material. Zircon trace element, Hf isotope and U/Pb isotope analyses were performed by laser-ablation ICP-MS. An in-house Archaean zircon standard yielded a $^{207}Pb/^{206}Pb$ age of 3465.1 ± 7.4 Ma (2 sd), which is in agreement with the published SHRIMP age of 3458 ± 2 Ma (Thorpe et al., 1992), and zircon reference material GJ-1 yielded a $^{206}Pb/^{238}U$ age of 610 ± 8 Ma (2 sd).

4. Petrography and field relationships

4.1. Bakhuis granulites

A representative selection of the granulite suite (15 samples, MKS 40 to 56) was sampled at Blanche Marie Falls (just north of the centre of the BGB, roughly 55 km NE from the Kabalebo airstrip; Fig. 1) and from drill core LA 156 taken from the centre of the Belt (approximately 35 km NE from the Kabelebo airstrip; Fig. 1). The BGB metamorphic suite can be subdivided into three groups: mafic granulites, intermediate granulites and metapelites. Both granulite groups are characterised by the presence of orthopyroxene and conspicuous compositional banding on the outcrop and hand sample scale. The mafic granulites have an equigranular mineral assemblage of plagioclase, hornblende, ortho- and clinopyroxene. Grain size and the relative proportion of hornblende are highly variable. The intermediate granulites are quartzofeldspatic orthopyroxene-bearing gneisses that contain quartz, plagioclase and in rare instances alkali-feldspar and less mafic minerals compared to the mafic granulites. Although orthopyroxene is invariably present, clinopyroxene and hornblende are absent from the more felsic samples in the intermediate group granulites, which comprise pegmatitic veins and leucosomes. The intermediate granulites have an equigranular texture, compositional banding and lack zoning and Karlsbad twinning in plagioclase.

A metapelitic, migmatised sillimanite gneiss (MKS 40) was sampled along the Kabalebo River. The outcrop in the middle of the river measures a couple of square metres, depending on the water level, and probably represents an isolated patch of the granulite suite within the charnockite body. The isoclinally folded melanosome of MKS 40 contains coarse sillimanite and sillimanite-biotite pseudomorphs after cordierite. Orthopyroxene is not observed and hence the characteristic UHT assemblage high-Al opx + sil + qtz is not present (e.g. Kelsey and Hand, 2014). The leucosome of MKS 40 has a coarse porphyritic texture and includes up to 3 cm large, euhedral mesoperthite. On the basis of its size and euhedral habit, we assert that the mesoperthite is magmatic and that its crystallisation temperature of 1025 °C (Fig. 3) indicates migmatisation under UHT conditions.

4.2. Kabalebo charnockites

The charnockites were sampled in the southwest part of the BGB, near the Kabalebo airstrip and western boundary shearzone. Due to the dense tropical rainforest, sampling locations are restricted to localised, deeply eroded outcrops in rivers and streams, making it difficult to determine field relationships. Nevertheless, 21 fresh charnockite samples were taken along the Kabalebo River, Zand Creek, Kilo Drie Creek and on the slopes of Misty Mountain (samples MKS 14–38; see supplementary material). On the outcrop scale, the charnockites are homogeneous and do not display compositional banding. At multiple localities, charnockite is seen in contact with gabbro, metadolerite and metagabbro. These mafic meta-igneous rocks are represented by rounded to angular hornblende-bearing metadolerite enclaves (5–150 cm) with an ophitic texture and larger bodies of coarse-grained metagabbro with poikilitic hornblende oikocrysts. Both these lithologies have a variable metamorphic overprint but primary magmatic textures are preserved, thereby clearly distinguishable from the BGB mafic granulites. On the basis of their magmatic texture and occurrence as enclaves within the charnockites, we interpret these metadolerite enclaves and metagabbroic bodies as comagmatic intrusives that are coeval with the charnockites. A suite of younger gabbroic bodies that lack a metamorphic overprint is also present in the BGB. Xenoliths of foliated mafic granulite with resorbed boundaries (5–50 cm) are abundant (up to 10% by volume) in the charnockites at some localities (Fig. 2b). The equigranular texture and clear foliation in these xenoliths is distinct from the metadolerite enclaves, but highly similar to the mafic granulites in the BGB, and hence we assert that these xenoliths represent either partly assimilated country rock or restites.

The Kabalebo charnockites have a porphyritic texture and a typical mineral assemblage of plagioclase, alkali-feldspar, ortho- and clinopyroxene, quartz and biotite (Fig. 2). Hornblende is present

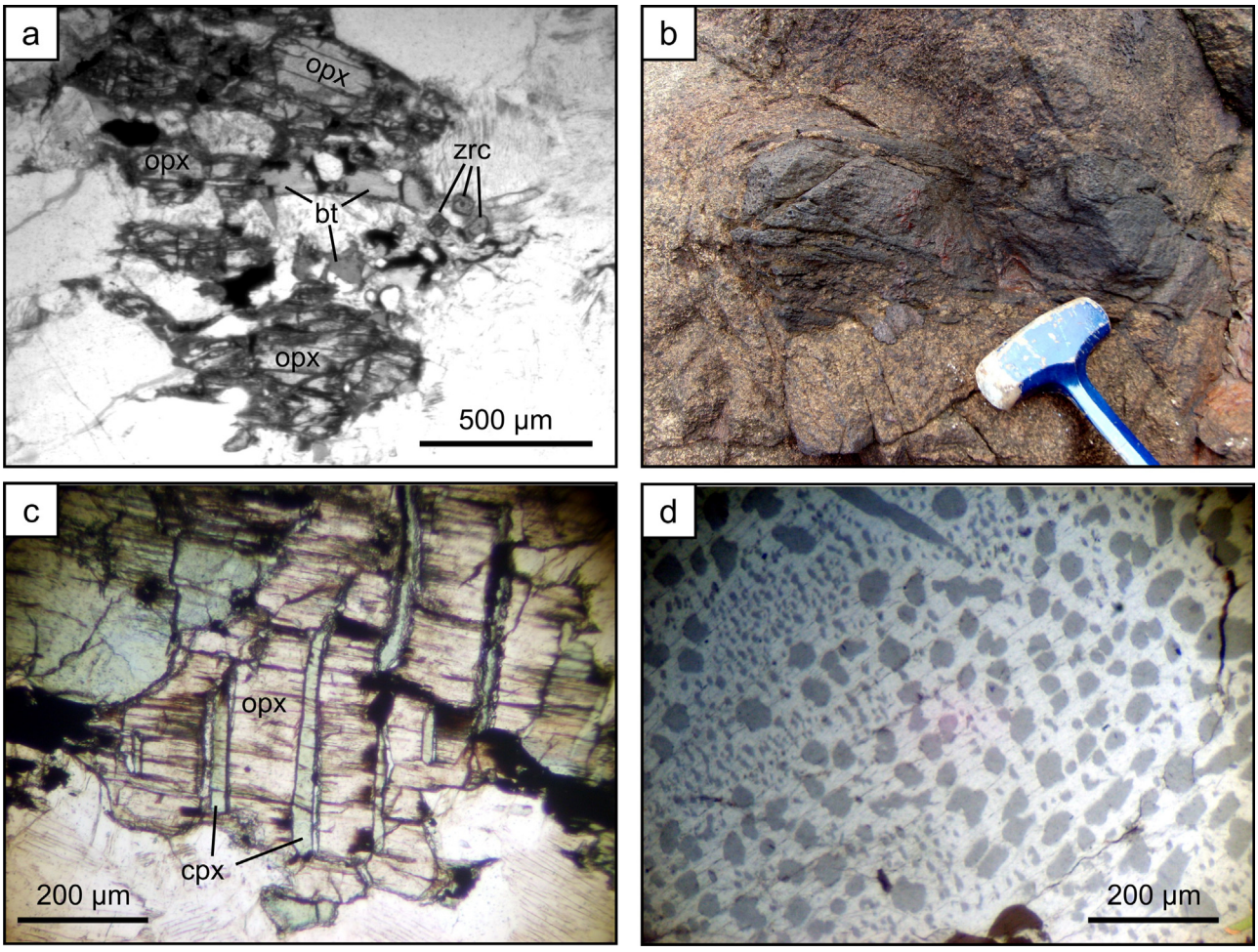

Fig. 2. Photomicrographs of charnockites. (a) Typical non-deformed charnockite texture with clusters of orthopyroxene and biotite in a feldspar-quartz matrix. The three zircon grains testify to the abundance of this mineral in the charnockites. (b) Resorbed mafic granulite xenolith at Krong Soela. Note the layering in the xenolith, which clearly distinguishes it from the metadolerite enclaves. (c) Inverted pigeonite: an orthopyroxene host with clinopyroxene exsolution lamellae, indicative of crystallisation temperatures >900 °C. (d) Coarse, patchy mesoperthitic exsolution in a sillimanite-gneiss leucosome.

only as a late interstitial phase or as local replacement of orthopyroxene. Apatite and zircon are common accessory phases and occur predominantly as inclusions in plagioclase. Fe–Ti-oxides are also copious but partly of secondary origin when they fill extensional veins related to mylonitisation. Up to 1 cm large plagioclase crystals are commonly euhedral, markedly zoned with antiperthitic rims and show Albite and Karlsbad twinning. Apparent crystal accumulation is visible in several samples where euhedral plagioclase grains form a brick-like fabric and zircon and apatite are relatively enriched. Due to the proximity to the western boundary shearzone, the samples have suffered variable deformation during the 1.2 Ga Nickerie event and magmatic textures have been partly obliterated. Nevertheless, the texture and microstructures of the Kabalebo charnockites are exclusively magmatic (Touret and Huizenga, 2012), and apart from the cataclasis the samples do not have a metamorphic overprint. The samples that are least effected by mylonitisation display typical features of high-temperature crystallisation. Anti-pertithic exsolution in plagioclase and mesoperthite are common features, and more rarely inverted pigeonite and blue Ti-rich quartz are present (Fig. 2). Two pigeonite grains in sample MKS 22 have similar Fe# (62.3 and 62.5), corresponding to a crystallisation temperature of 960 °C. A total of six ternary feldspar grains from two samples yield temperatures similar to the pigeonites. Three out of four grains from sample MKS 30 indicate crystallisation at 970 °C, sample MKS 22 suggests an even higher temperature around 990 °C (Fig. 3).

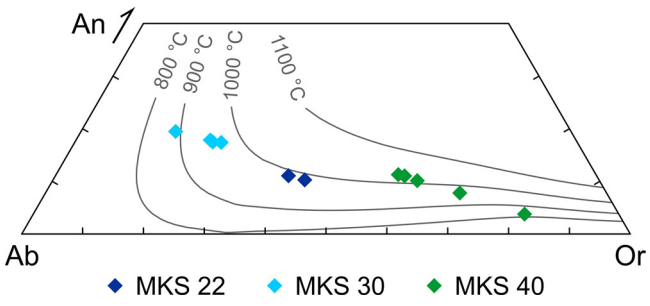

Fig. 3. Mesoperthite geothermometry of Kabalebo charnockite samples (MKS 22 and MKS 30) and leucosome of a sillimanite-gneiss (MKS 40). Isotherms calculated using the Fuhrman and Lindsley (1988) model at 0.85 GPa. Mesoperthite in the charnockites yields crystallisation temperatures of 960–990 °C, the sillimanite-gneiss indicates migmatisation under UHT conditions at a peak temperature of ~1025 °C.

5. Results

5.1. Geochronology

5.1.1. Kabalebo charnockites

Zircon fractions of the five charnockite samples yielded homogeneous populations of sub- to euhedral, transparent pale yellow 50–400 µm long crystals with aspect ratios of 3:1 to 6:1. The

zircons show light to dark blue cathode luminescence (CL) colours of variable brightness. In CL and BSE images (Fig. 4; additional images provided in the online supplementary material), the majority have a typical magmatic texture with oscillatory and/or sector zoning but CL dark, unzoned grains are also present. There is no clear correlation between CL/BSE texture and crystal morphology. Acicular apatite inclusions occur in roughly half of the zircon grains. Evidence for punctuated growth of zircon is provided by the frequent presence of internal resorption boundaries. Although resorption can occur during magmatic growth (Hoskin and Schaltegger, 2003), grains with complex resorption boundaries were avoided for analysis. Individual zircon dates are (sub)concordant and are displaced from the concordia along an elemental fractionation vector, i.e. they lie on constant $^{207}Pb/^{206}Pb$ lines. Therefore, weighted average $^{207}Pb/^{206}Pb$ ages of 34–47 individual analyses per sample are reported for the charnockite samples (Fig. 4 and supplementary material). All errors are at the 95% confidence level including the uncertainty on uranium decay constants.

Charnockites MKS 19 and 22 from two sampling localities on Misty Mountain represent the least mylonitised samples and have retained original magmatic textures. Inverted pigeonite and mesoperthitic feldspar in MKS 22 are used for thermometry (see Section 4). These two charnockite samples yield $^{207}Pb/^{206}Pb$ ages of 1984.4 ± 3.9 Ma and 1991.2 ± 3.5 Ma respectively. Charnockite MKS 26 is sampled at the Krong Soela rapid, close to the western boundary shearzone of the BGB, where restitic mafic granulite xenoliths are abundant. Zircons from MKS 26 are characterised by the common presence of thin, CL dark rims around slightly rounded, very mildly resorbed cores. Unfortunately, these rims proved to be too thin for LA analysis and only the magmatically zoned cores have been dated and yield a $^{207}Pb/^{206}Pb$ age of 1992.5 ± 4.5. Charnockite MKS 36 from the Zand Creek yielded the most pristine zircons that on average show the brightest CL. Petrography and whole rock geochemistry point to accumulation of zircon in this sample though crystal fractionation (see Section 6.2.2). Due to relatively low U-content in these early formed zircons, individual $^{207}Pb/^{206}Pb$ dates have larger uncertainty compared to the other samples. Nevertheless, analysis of 47 grains from this sample yielded a $^{207}Pb/^{206}Pb$ age of 1987.0 ± 6.3 Ma. Charnockite MKS 38 is sampled ~10 m away from a large body of metagabbro at the Moi-Moi waterfall. Zircon from this sample is similar to other samples, although ~10% of the grains have a thin, CL-dark rim that is seen more frequently in sample MKS 26. The $^{207}Pb/^{206}Pb$ age of sample MKS 38 is 1988.0 ± 4.3 Ma. To summarise: the five Kabalebo charnockite samples yield $^{207}Pb/^{206}Pb$ ages indistinguishable within analytical error of each other that range from 1984.4 to 1992.5 Ma.

5.1.2. Sillimanite gneiss

Zircon was extracted from a ~10 cm thick leucosome of sillimanite gneiss sample MKS 40, which is described in more detail in Section 4.1. The inclusion of some mm-wide melanosomes could not be avoided. Compared with the charnockite samples, zircon from the sillimanite-gneiss is more stubby and yellow in colour. Cathode luminescence is restricted to faint dark blue colours. BSE images indicate the presence of two distinct zircon populations in this sample. Population A contains sub- to euhedral grains with oscillatory and sector zoning, typical of magmatic zircon, while population B comprises more rounded grains. The main distinguishing feature, however, is the presence of a BSE mid-grey, unzoned, featureless rim around resorbed cores in population B (Fig. 4). Our interpretation is that population MKS 40-A represents zircon that formed in the leucosome as a result of migmatisation during UHT metamorphism. Zircons from population MKS 40-B are interpreted as inherited grains from the protolith of the sillimanite gneiss. These zircons are probably derived from the melanosome and experienced resorption and metamorphic growth during UHT metamorphism, leading to the development of the unzoned, mid-grey rims. Both populations typically have a very thin, slightly resorbed outer rim of only a few μm thick, which surrounds the metamorphic rim in MKS 40-B and hence appears to represent a younger phase of zircon growth. Unfortunately, only the resorbed, magmatically zoned cores of MKS 40-B could be dated as the mid-grey, metamorphic rims were almost always too thin for LA analysis. Low U-content of MKS 40 zircons led to low count rates for ^{235}U and ^{207}Pb during analysis and hence large errors on $^{207}Pb/^{235}U$ and $^{207}Pb/^{206}Pb$ ratios. Therefore, weighted average $^{206}Pb/^{238}U$ ages are reported for the two populations in this sample (Fig. 4). A weighted average of 34 $^{206}Pb/^{238}U$ dates of MKS 40-A zircon gives an age of 2072.6 ± 7.3 Ma, which is in good agreement with the 2055–2072 Ma zircon Pb–Pb evaporation ages for the UHT metamorphism reported by De Roever et al. (2003). The magmatically zoned, resorbed cores of MKS 40-B zircon yield a $^{206}Pb/^{238}U$ age of 2131 ± 11 Ma. The high MSWD of 2.1, however, suggests that this is not a single zircon population but a mix of detrital zircons with an age range of roughly 2120–2150 Ma.

5.2. Whole rock geochemistry

5.2.1. Major elements

A summary of the whole rock Sr–Nd isotope, major and trace element composition of representative charnockite and granulite samples is given in Table 1. The full dataset is available in the online supplementary material. Major element variation of the Kabalebo charnockites, mafic and intermediate granulites and metagabbroic samples (metagabbro and metadolerite enclave) is depicted against SiO_2 wt.% in Fig. 5. The charnockite suite displays a relatively wide range in silica-content from 56 to 74 wt.% SiO_2 and comprises tonalites, granodiorites and granites. The majority of the samples has >64 wt.% SiO_2, while four samples have intermediate SiO_2 contents between 56 and 61 wt.% and are tonalitic in composition. Most major elements show clear negative correlations with silica content with the exception of K_2O that increases with SiO_2 and Na_2O that is more variable. The majority of the samples are magnesian, calc-alkalic, metaluminous charnockites while some of the evolved samples are mildly peraluminous and alkali-calcic or mildly ferroan (Frost et al., 2001; Frost and Frost, 2008). The field distinction between mafic and intermediate granulites is corroborated by their major element composition. Intermediate granulites have SiO_2 contents between 53 and 64 wt.% with felsic members of the intermediate granulite group such as pegmatitic veins ranging up to 79 wt.% SiO_2 (Fig. 5). Major element concentrations of the intermediate granulites generally overlap with the charnockite trends, but potassium contents are markedly different. The charnockite suite ranges from 2 to 6 wt.% K_2O while the intermediate granulites do not exceed 2 wt.%. In addition, TiO_2 and P_2O_5 contents of the intermediate granulites are consistently lower than in the charnockites. The metagabbroic samples and mafic granulites define a narrow SiO_2 range from 48 to 51 wt.%, but are highly heterogeneous in terms of other major elements. For example, MgO varies between 5 and 13 wt.%.

5.2.2. Trace elements

Variation of a selection of diagnostic trace elements with silica content is displayed in Fig. 6. Most trace elements show a marked decrease in concentration with SiO_2 content. Notable variation is present within the four intermediate charnockites (56–61 wt.% SiO_2) and these samples generally do not fall on the differentiation trend defined by the main charnockite suite. Strontium concentration varies between ~200 and ~500 ppm for the main charnockite group, but ranges up to ~1000 ppm in one intermediate charnockite. High field strength elements (HFSE) decrease with SiO_2 wt.%, but show marked scatter as exemplified by zirconium (Fig. 6). In

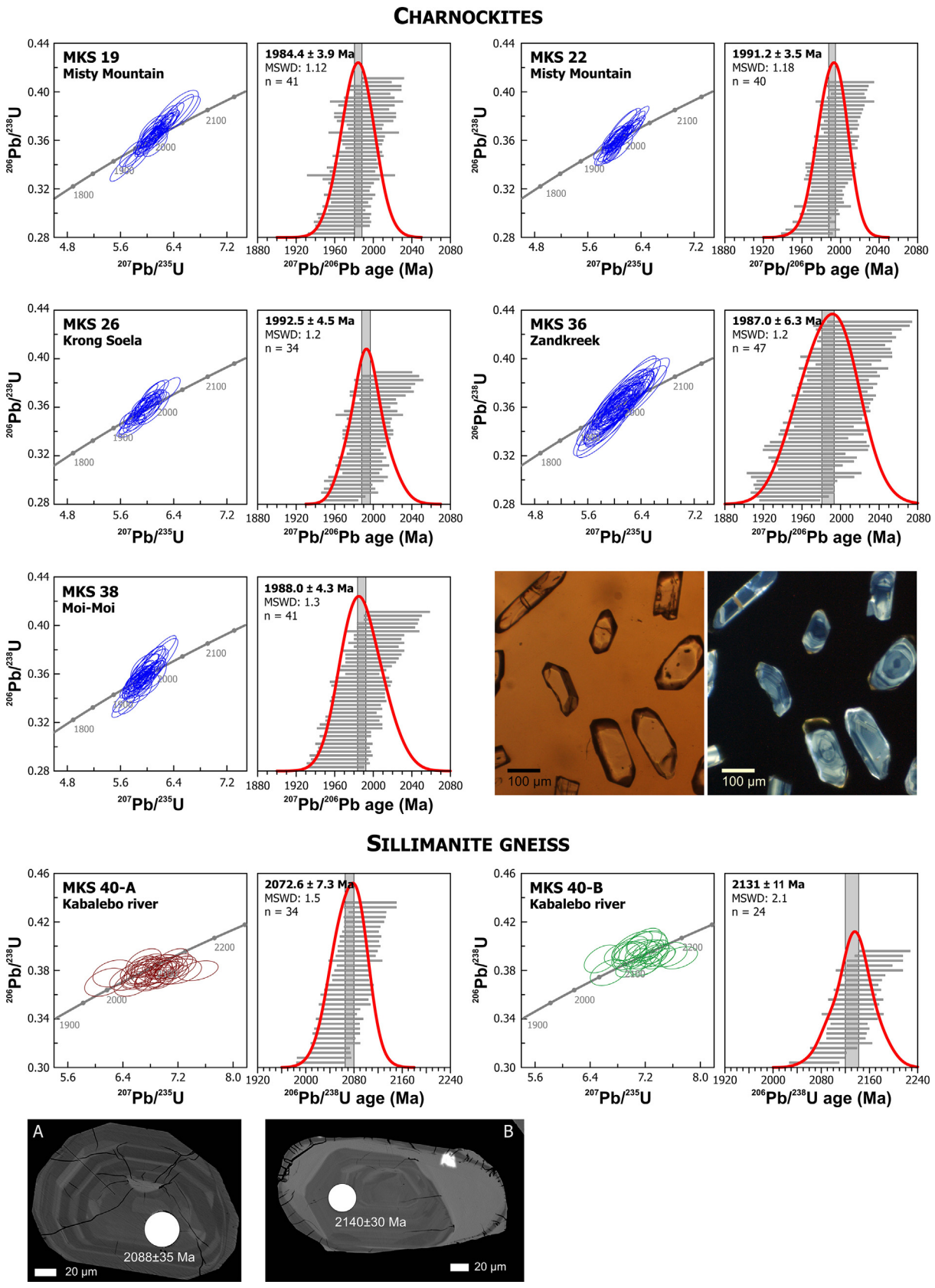

Fig. 4. Results of the U–Pb dating of BGB zircon. Five charnockite samples yield $^{207}Pb/^{206}Pb$ ages within error of each other ranging from 1984 to 1993 Ma, which is clearly younger than the UHT metamorphism as demonstrated by a 2073 Ma age for a sillimanite-gneiss. An inherited population in the latter sample yields an age spectrum of roughly 2120–2150 Ma. See text for further discussion. Additional CL and BSE images of the dated zircons are provided in the online supplementary material.

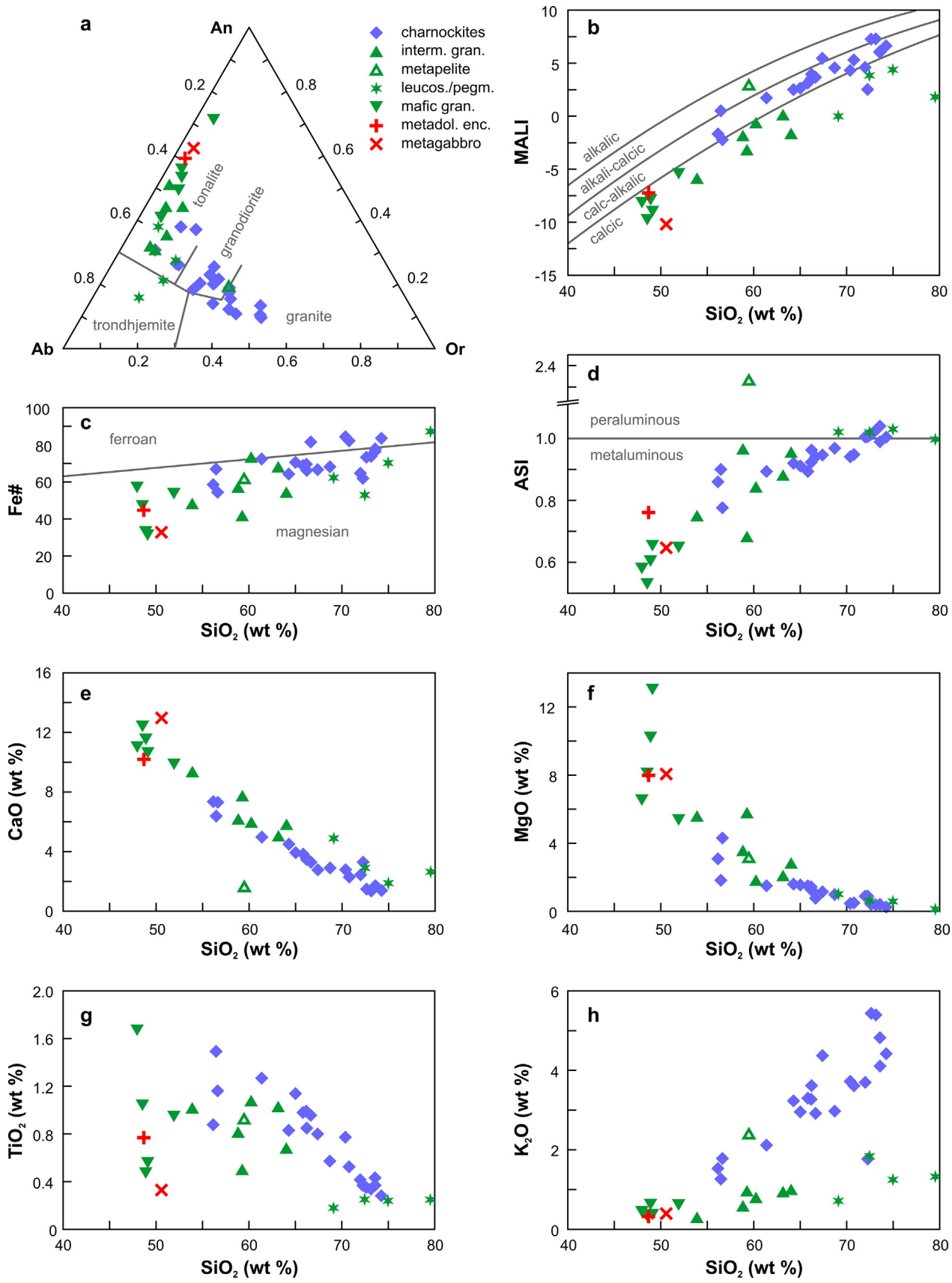

Fig. 5. Variation of selected major element parameters with silica-content of the Kabalebo charnockites and BGB granulite suite. Modified alkali-lime index (MALI), aluminium saturation index (ASI) and Fe# (molar Fe/(Fe + Mg)) after Frost et al. (2001). The majority of the Kabalebo charnockites are magnesian, metaluminous and calc-alkalic, similar to most other charnockites associated with (U)HT metamorphic terrains.

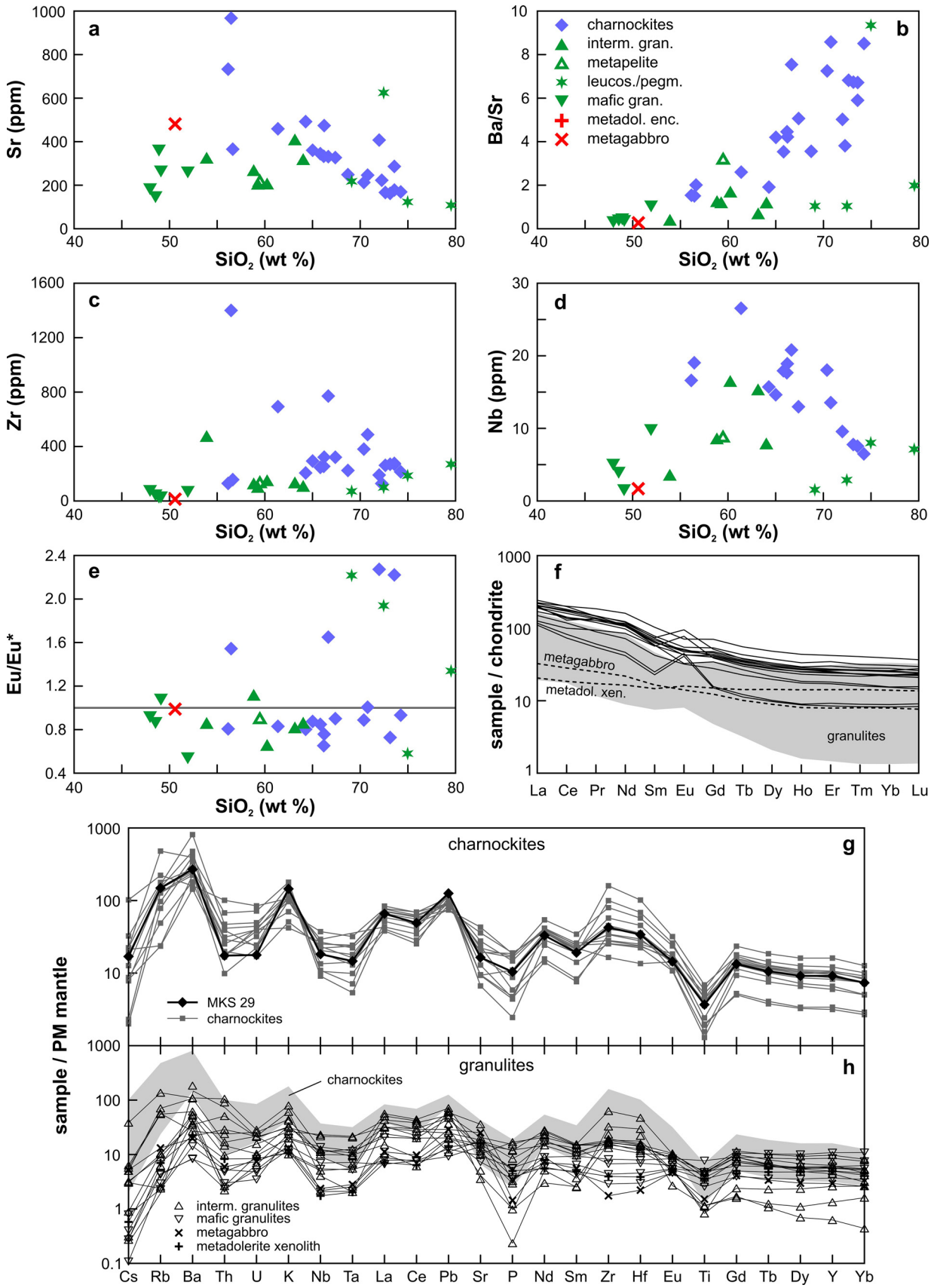

Fig. 6. Trace element variation of the Kabalebo charnockites and BGB granulite suite. Europium anomaly is calculated as $Eu_N/\sqrt{(Sm_N \times Gd_N)}$, where the subscript "*N*" denotes chondrite normalised values. Rare earth element patterns are normalised to C1 chondrite values from McDonough and Sun (1995), multi-element variation diagrams are normalised to primitive mantle values from Sun and McDonougy (1989). Sample MKS 29 is highlighted as a typical primitive charnockite, see text for further discussion.

Table 1
Whole rock Sr–Nd isotope, major and trace element composition of representative charnockite and granulite samples.

Sample Lithology	MKS 19 char	MKS 22 char	MKS 25 char	MKS 26 char	MKS 29 char	MKS 30 char	MKS 36 char	MKS 38 char	MKS 40 metap	MKS 44 maf gran	MKS 45 int gran	MKS 51 maf gran	MKS 54 int gran
SiO_2	73.87	69.86	55.89	71.88	66.22	65.83	55.31	59.29	58.83	48.29	62.13	47.98	59.14
TiO_2	0.28	0.52	0.87	0.42	0.79	0.94	1.46	1.23	0.92	0.55	1.01	1.03	1.06
Al_2O_3	13.20	13.60	18.29	13.23	14.77	14.47	19.18	15.91	20.53	13.96	14.62	13.94	15.62
FeO	2.26	4.06	7.81	2.21	4.04	6.05	6.51	6.85	9.15	10.53	8.01	12.90	8.97
MnO	0.04	0.08	0.16	0.05	0.09	0.14	0.20	0.17	0.12	0.19	0.13	0.25	0.14
MgO	0.25	0.49	3.07	0.38	1.13	0.76	1.79	1.45	3.13	12.81	2.07	8.00	1.80
CaO	1.39	2.26	7.32	1.68	2.73	3.25	6.25	4.81	1.64	10.45	4.98	12.26	5.88
Na_2O	3.60	3.95	4.14	2.85	3.80	4.01	5.51	4.43	2.18	1.25	4.20	2.28	4.50
K_2O	4.40	3.56	1.52	4.71	4.30	2.88	1.24	2.05	2.38	0.36	0.93	0.32	0.79
BaO	0.17	0.24	0.12	0.19	0.19	0.28	0.16	0.13	0.08	0.01	0.03	0.01	0.04
P_2O_5	0.05	0.10	0.41	0.10	0.22	0.19	0.40	0.36	0.06	0.08	0.33	0.08	0.36
LOI	0.15	0.16	0.13	0.46	0.22	0.09	0.17	0.35	0.34	0.37	0.53	0.24	0.10
Sum	99.65	98.88	99.74	98.17	98.51	98.90	98.19	97.02	99.36	98.85	98.98	99.29	98.38
Li	3.50	15.72	22.93	14.61	18.62	18.77	12.28	23.14	25.64	11.40	8.59	17.94	12.25
Be	1.11	1.44	2.74	0.96	1.42	1.56	1.84	2.76	0.64	0.29	2.10	0.76	1.64
Sc	4.58	7.63	32.36	5.70	20.67	29.59	16.73	15.78	33.86	44.19	31.02	54.01	23.62
V	11.22	21.03	170.56	17.83	61.50	28.98	65.38	58.18	189.95	217.73	98.82	341.80	111.70
Cr	3.21	4.62	46.22	4.41	16.71	6.53	2.13	7.53	228.37	1171.19	14.56	191.97	5.13
Co	2.51	4.65	25.67	3.25	9.98	8.60	6.95	11.03	40.95	70.00	19.71	60.13	25.31
Ni	1.86	3.15	17.03	2.19	8.88	5.00	3.72	4.12	107.68	395.51	16.96	106.61	11.95
Cu	4.49	10.33	50.88	7.67	21.45	14.42	19.48	19.81	9.00	232.49	206.50	43.39	57.83
Zn	40.65	71.37	88.90	31.81	68.16	106.50	120.00	128.46	105.93	71.83	114.65	119.01	86.81
Ga	17.70	19.39	23.96	15.67	19.25	21.73	22.94	24.04	30.09	14.65	25.18	17.53	20.36
Rb	80.79	49.59	14.92	112.75	94.45	61.52	15.10	31.06	86.58	1.47	6.67	2.83	3.97
Sr	140.3	200.2	757.2	272.0	346.2	345.2	905.5	467.0	244.1	295.1	437.1	153.8	216.1
Y	27.18	39.28	45.95	14.34	41.65	37.39	46.20	73.20	20.10	16.79	28.65	27.34	44.28
Zr	283.4	642.4	184.4	385.0	476.9	1117.6	1787.3	893.1	203.8	32.2	168.8	49.0	188.3
Nb	6.48	13.55	16.61	7.55	12.99	20.80	19.04	26.55	8.86	1.48	15.38	3.89	16.54
Cs	0.07	0.06	0.26	1.04	0.54	0.25	0.68	0.28	1.23	0.03	0.03	0.01	0.01
Ba	1563.7	2391.0	1001.0	1893.7	1877.5	2803.4	1570.4	1268.9	765.1	99.3	246.2	57.8	361.0
La	35.40	46.70	48.42	26.15	45.14	29.74	40.08	53.19	38.64	6.00	29.59	5.40	22.00
Ce	72.34	83.23	104.56	44.88	87.21	61.16	86.50	122.88	78.34	13.27	67.91	14.01	52.77
Pr	8.27	11.86	12.82	5.06	11.13	8.73	11.86	17.19	9.37	1.78	8.15	2.05	6.66
Nd	32.81	48.33	49.74	19.10	44.62	38.78	53.03	73.33	35.95	7.91	31.62	9.55	27.98
Sm	6.25	9.25	9.78	3.37	8.50	8.37	10.93	15.25	6.60	2.04	6.57	2.89	6.49
Eu	1.80	2.88	2.40	2.31	2.43	4.35	5.35	3.98	1.76	0.77	1.68	0.92	1.45
Gd	5.54	8.23	8.37	2.99	7.94	7.71	10.20	13.97	5.34	2.35	5.96	3.69	6.89
Tb	0.82	1.17	1.23	0.41	1.14	1.09	1.36	2.00	0.70	0.39	0.86	0.65	1.09
Dy	4.85	6.93	7.22	2.40	6.74	6.32	7.81	11.84	3.61	2.62	5.00	4.35	6.80
Ho	0.96	1.36	1.46	0.48	1.37	1.27	1.56	2.38	0.67	0.56	0.93	0.94	1.42
Er	2.74	3.85	4.19	1.36	3.96	3.58	4.37	6.75	1.82	1.68	2.54	2.73	4.14
Tm	0.39	0.58	0.66	0.20	0.57	0.54	0.65	1.00	0.26	0.27	0.37	0.43	0.64
Yb	2.47	3.67	4.15	1.32	3.63	3.64	4.19	6.24	1.54	1.72	2.26	2.71	4.03
Lu	0.36	0.56	0.60	0.20	0.55	0.58	0.68	0.91	0.24	0.25	0.31	0.39	0.58
Hf	6.91	14.03	4.18	9.12	10.49	21.10	31.37	17.69	4.65	0.92	3.92	1.41	4.35
Ta	0.22	0.53	0.67	0.41	0.60	n.d.	0.91	1.31	0.38	0.09	0.84	0.22	0.89
W	0.12	0.16	0.17	0.22	0.19	0.15	0.35	0.29	0.06	0.06	0.16	0.16	0.13
Tl	1.35	1.05	0.47	1.97	1.59	1.08	0.38	0.75	1.27	0.20	0.25	0.08	0.14
Pb	21.30	18.03	13.70	20.60	23.22	17.34	13.77	16.70	13.13	1.70	9.67	3.72	8.73
Bi	0.01	0.00	0.02	0.03	0.02	0.02	0.04	0.03	0.00	0.01	0.09	0.31	0.13
Th	2.48	3.31	1.68	3.52	1.48	1.42	2.15	1.51	8.98	0.45	4.33	0.41	0.82
U	0.51	0.48	0.36	0.93	0.37	0.88	0.84	0.80	0.60	0.10	0.44	0.17	0.33
$^{87}Sr/^{86}Sr$	0.74119	0.72263	0.70583	0.73517	0.72587	0.71712	0.70419	0.70961	0.73229	0.70281	0.70519	0.70387	0.70472
$^{87}Rb/^{86}Sr$	1.6716	0.7175	0.0570	1.2027	0.7907	0.5161	0.0482	0.1925	1.0287	0.0144	0.0442	0.0532	0.0531
$(87Sr/^{86}Sr)_i$	0.6936	0.7022	0.7042	0.7010	0.7034	0.7024	0.7028	0.7041	0.7030	0.7024	0.7039	0.7024	0.7032
$^{143}Nd/^{144}Nd$	0.51153	0.51155	0.51163	0.51148	0.51160	0.51177	0.51169	0.51173	0.51151	0.51215	0.51163	0.51253	0.51186
$^{147}Sm/^{144}Nd$	0.1152	0.1156	0.1188	0.1067	0.1151	0.1305	0.1245	0.1257	0.1110	0.1555	0.1256	0.1829	0.1402
$(^{143}Nd/^{144}Nd)_i$	0.51003	0.51005	0.51008	0.51009	0.51011	0.51008	0.51007	0.51010	0.51007	0.51013	0.50999	0.51016	0.51004
TDM [Ga]	2.34	2.31	2.27	2.22	2.22	2.32	2.32	2.27	2.26	2.33	2.45	2.55	2.45

Abbreviations: char: charnockite; metap: metapelite; int gran: inter.

multi-element variation diagrams, the charnockites have uniform patterns similar to average continental crust (Fig. 6) but are characterised by pronounced mobile element depletion as demonstrated by relative depletion of U, Rb, Cs and Th (Th being mobile in halogen rich, H_2O-poor fluids; see Section 6.1). In contrast, Ba, P, Ti, Zr and REE are relatively more abundant than average continental crust. Both the enrichment in HFSE, P, Ti, Ba and mobile element depletion are common in magnesian, calc-alkalic charnockites in granulite terrains (e.g. Kilpatrick and Ellis, 1992; Zhao et al., 1997). The granulite suite has a similar trace element fingerprint to the charnockites but on average lower absolute trace element concentrations. Mobile element depletion, highly characteristic for the Kabalebo charnockites, is also present in the granulites. Pegmatitic veins and leucosomes (>65 wt.% SiO_2) in the granulite suite have low trace element concentrations and trough-shaped REE patterns. The mafic granulites and metagabbroic rocks fall predominantly in the island arc tholeiite field in trace element discrimination plots.

5.2.3. Radiogenic isotopes

Strontium and neodymium isotope compositions were determined on a selection of charnockite and granulite samples (Fig. 7). Initial ε_{Nd} at 1985 Ma of charnockites and granulites is highly uniform and most samples are within error and close to bulk Earth values. Neodymium depleted mantle model ages (DePaolo, 1981) of the charnockite suite are between 2.22 and 2.34 Ga (Fig. 7b). Strontium isotope composition and Rb/Sr ratios are more variable and initial $^{87}Sr/^{86}Sr$ ranges from 0.701 to 0.705. The granulites are very similar and have $^{87}Sr/^{86}Sr$ between 0.702 and 0.7045, while ε_{Nd} displays a slightly larger spread from +2 to −2 compared to the charnockites, albeit all samples are within analytical error. The

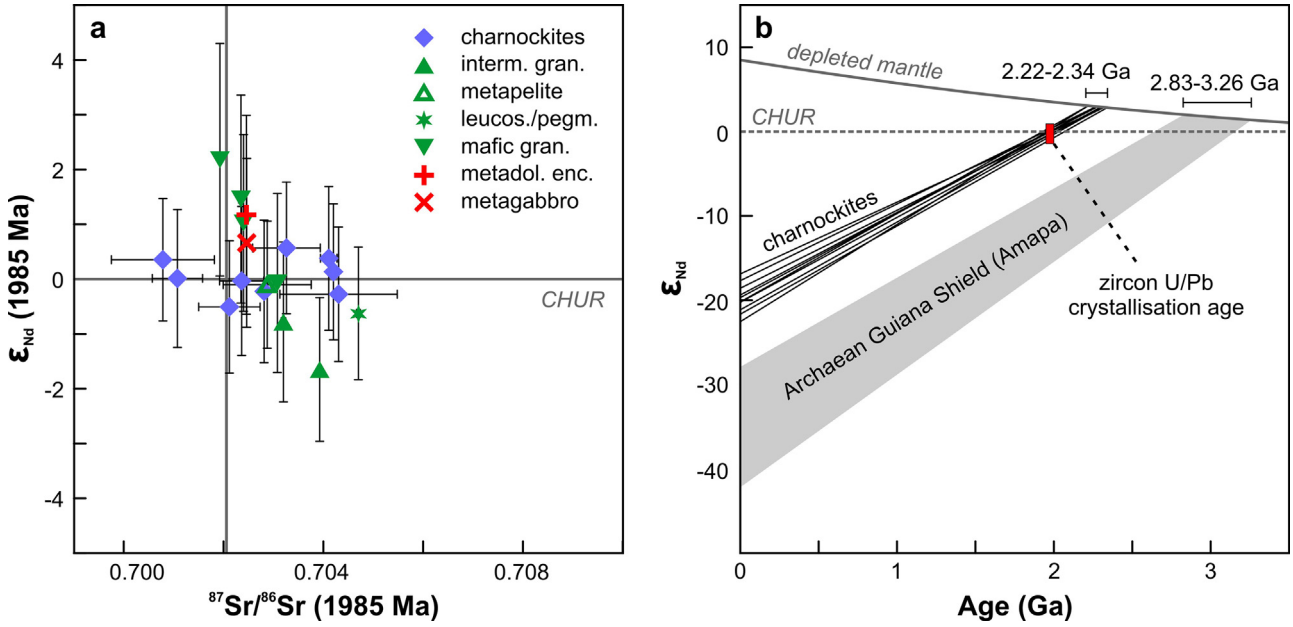

Fig. 7. Sr–Nd isotope variation of the Kabalebo charnockites and BGB granulite suite. (a) Initial $^{87}Sr/^{86}Sr$ and ε_{Nd} at time of crystallisation (1985 Ma) are within error of bulk Earth values and do not differ significantly between sample groups, partly due to large propagated errors; (b) depleted mantle neodymium model ages (DePaolo, 1981) of the Kabalebo charnockites (~2.3 Ga) exclude the involvement of Archaean material in their genesis. The range in Nd model ages of the Archaean Amapa block is plotted for comparison (da Rosa-Costa et al., 2006).

Sr–Nd data of the Bakhuis granulites are in agreement with previous studies that quote ca. 2.3 Ga Nd model ages and initial $^{87}Sr/^{86}Sr$ of ca. 0.705 (De Roever et al., 2003; Priem et al., 1971).

5.3. Zircon geochemistry

5.3.1. Trace element composition

The full dataset of zircon trace element and Hf isotope composition is given in the online supplementary material. Rare-earth element patterns of Kabalebo charnockite zircons are typical of magmatic zircon with steeply increasing REE concentrations from La to Lu, large positive cerium and moderate negative europium anomalies. Significant rare-earth element variation is present and LREE–MREE concentrations vary by more than an order of magnitude within a sample. Rare-earth element slopes, however, are more uniform and inter-sample variation is limited.

The Zr/Hf ratio in zircon is shown to decrease with progressive fractional crystallisation of zircon (e.g. Claiborne et al., 2006; Linnen and Keppler, 2002). Hafnium content in zircon can therefore be used as a proxy for melt evolution and hence trace-element concentration in Kabalebo zircon is plotted against Hf in Fig. 8. Hafnium content ranges between 6500 and 11,000 ppm and is positively correlated with whole rock SiO_2 wt.%: the most primitive zircon grains (lowest Hf) reside in the most mafic samples. The uranium content of the Kabalebo zircons is low compared to average zircon (Hoskin and Schaltegger, 2003) and it varies between 40 and 300 ppm with >80% of the samples below 150 ppm. The increase of U (and Th) with melt evolution suggests that no U-rich minerals have co-precipitated with zircon. U/Th ratios range from 0.6 to 2.4, typical of igneous zircon, and show a moderate positive correlation with Hf-content. Sample MKS 36 plots at consistently lower U/Th ratios compared to the main trend. Rare-earth element concentrations decrease with hafnium and U/Th ratio (not shown) and the REE-slope becomes steeper (higher Lu/Sm). Niobium concentrations range from ~2.5 to ~13 ppm and are positively correlated with Hf. Europium anomalies (Eu/Eu^*) become larger with hafnium content from ~0.6 to <0.06. Coeval fractionation of plagioclase will preferentially deplete the melt in Eu, leading to a larger Eu-anomaly in zircon. Titanium content is negatively correlated with Hf and ranges from 5 to 30 ppm. Assuming a TiO_2-activity of 0.7 and silica-activity of 1, this yields Ti-in-zircon crystallisation temperatures between 750 and 950 °C (Ferry and Watson, 2007). The Ti-in-zircon temperatures display a bimodal distribution with peaks at 750–775 °C and 850–875 °C that is characteristic of all individual samples, and correlate with hafnium-, uranium- and REE-concentrations and Eu-anomaly (Fig. 8). Ti-in-zircon crystallisation temperatures are more than 100 °C lower than charnockite crystallisation temperatures obtained from pigeonite and mesoperthite. Moreover, average temperatures per sample are also ~50 °C lower than whole rock zircon saturation temperatures (Watson and Harrison, 1983). This discrepancy may result from a choice of Ti-activity that is too high. Titanium-activity is notoriously difficult to quantify, but a value of <0.3 is required to raise the highest Ti-in-zircon temperatures to ~960 °C, which appears improbably low given the abundance of Fe–Ti-oxides and high whole rock Ti-content.

5.3.2. Hafnium isotopes

Measured hafnium isotope compositions of the Kabalebo zircons were age corrected using a decay constant of 1.865×10^{-11} (Scherer et al., 2001) and their $^{207}Pb/^{206}Pb$ crystallisation ages (see Section 5.1.1). No within-grain core to rim $^{176}Hf/^{177}Hf$ variation was observed. Oscillatory Lu and Yb zoning is visible when Lu/Hf and Yb/Hf ratios are plotted against laser-ablation pit depth, but hafnium content (represented by the ^{176}Hf signal intensity) and isotope composition are homogeneous. Growth zones with distinct Lu/Hf ratios were processed individually but yielded $^{176}Hf/^{177}Hf$ ratios that are identical within error. We conclude that the variable within-grain Lu/Hf ratios have no influence on the age corrected ε_{Hf} values. The initial Hf isotope composition of the zircons is remarkably homogeneous with no inter-sample variation. The total range in initial ε_{Hf} for the five samples, excluding one outlier at $\varepsilon_{Hf} = 4.8$, is less than 4 epsilon units ($\varepsilon_{Hf} = -1.8$–2.0). If the internal precision of the individual measurements is used, the total population shows a slightly skewed probability density plot with a weighted average initial ε_{Hf} of -0.02 ± 0.20 and an MSWD of 2.2. When the reproducibility of the GJ-1 standard is employed (± 1.8 ε_{Hf} units),

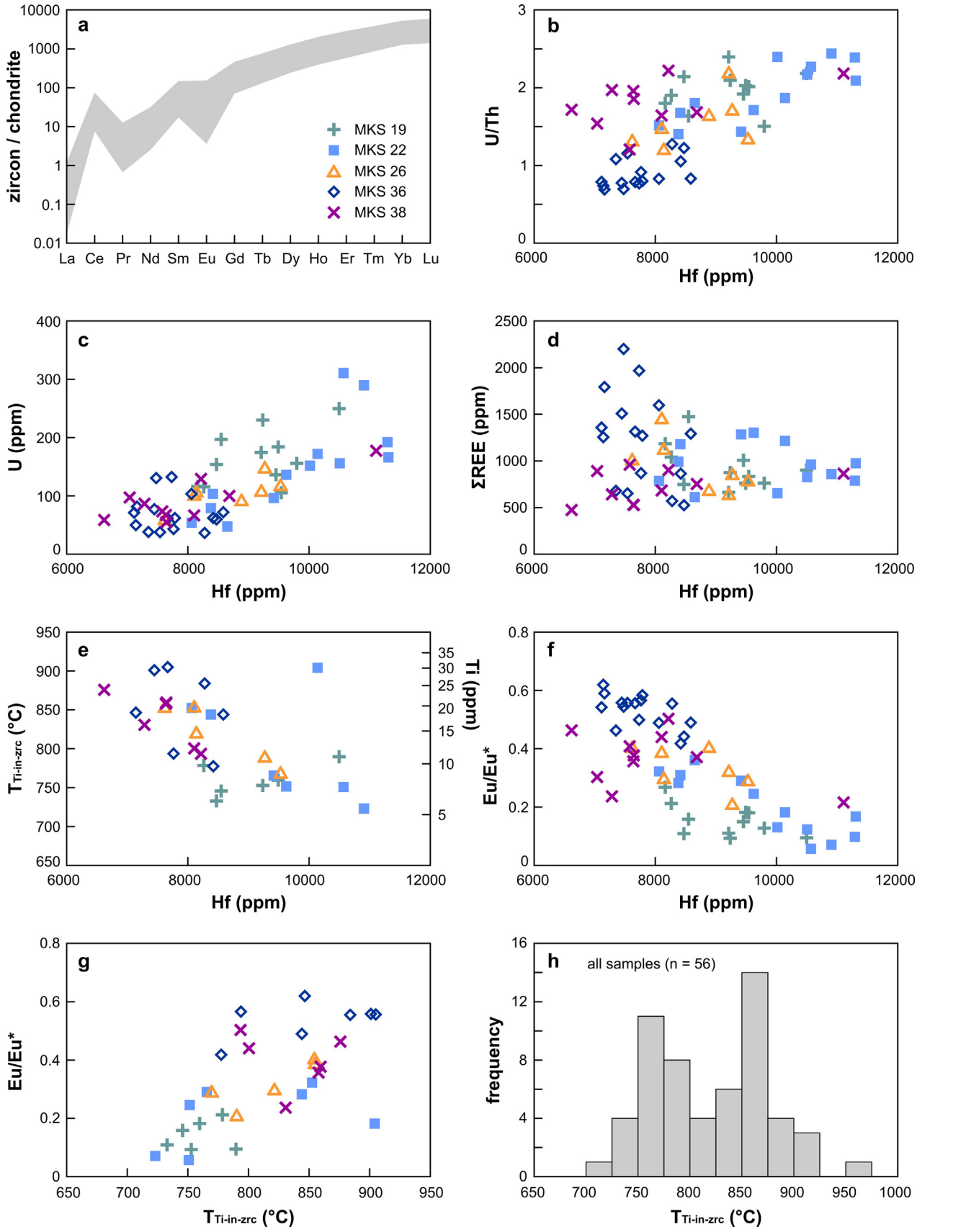

Fig. 8. Trace element variation of zircons from the Kabalebo charnockites. Hafnium concentration is used a proxy for melt evolution with Hf increasing with differentiation. Europium anomaly is calculated as $Eu_N/\sqrt{(Sm_N \times Gd_N)}$, subscript "*N*" denotes chrondrite normalised values (McDonough and Sun, 1995). Titanium-in-zircon temperatures are calculated using the Ferry and Watson (2007) calibration with a silica activity of 1 and Ti-activity of 0.7. See text for further discussion.

the samples display a perfect Gaussian distribution with a weighted average of −0.08 ± 0.21 and an MSWD of 0.90. Zircon Hf model ages were calculated using the depleted mantle composition of Scherer et al. (2001), recalculated to CHUR values of Bouvier et al. (2008), assuming a crustal $^{176}Lu/^{176}Hf$ ratio of 0.011 (Rudnick and Gao, 2003). Model ages vary from 2.10 to 2.44 Ga with a peak at 2.34 Ga.

6. Discussion

6.1. The source of the Kabalebo charnockites

One of the main geochemical characteristics of the Kabalebo charnockites is a depletion in the mobile elements Cs, Rb, U and Th. Although Th normally behaves as an immobile element, its mobility drastically increases in halogen-rich fluids, which are liberated upon the breakdown of micas during prograde metamorphism (Keppler and Wyllie, 1990). The lack of a pervasive metamorphic overprint in the Kabalebo charnockites, in combination with their relatively high K_2O content, suggests that the mobile element depletion is inherited from the source and not the result of later metamorphic dehydration. This is corroborated by the predominance of primary magmatic orthopyroxene over hornblende, which indicates that the charnockitic melt was relatively anhydrous. The second conspicuous feature of the Kabalebo charnockites is high TiO_2, P_2O_5, K_2O, Ba, REE and Zr contents compared to average granites. This geochemical fingerprint is similar to other magnesian, calc-alkalic charnockites (e.g. Kilpatrick and Ellis, 1992; Young et al., 1997; Zhao et al., 1997) and reflects the source and melting conditions of the Kabalebo charnockites. The high K_2O and incompatible trace element concentrations preclude a source that has experienced a previous episode of melt extraction. To account for the inherited mobile element depletion, however, a dehydrated source is required. Dehydration of the protolith of the charnockites prior to melting is an effective mechanism to remove Cs, Rb, U and Th. Depletion of the alkalis and U–Th is a characteristic feature of granulite terrains (Rudnick and Presper, 1990) and hence dehydrated but fertile granulites appear to be a suitable source for the Kabalebo charnockites. Melting of an anhydrous source requires higher temperatures than for dehydration or wet melting, which is corroborated by >950 °C crystallisation temperatures of the Kabalebo charnockites. The characteristic TiO_2, P_2O_5 and Zr enrichment is also favoured by high-temperature melting as the solubility of refractory phases such as apatite, ilmenite and zircon increases with temperature (e.g. Harrison and Watson, 1984; Watson and Harrison, 1983). The lack of inherited grains in the ca. 300 zircons analysed for U/Pb dating in this study also suggests that the charnockitic melt was undersaturated in Zr. Relatively cold granites are often saturated in Zr, P and other trace elements hosted in refractory phases, as indicated by the common occurrence of inherited zircon xenocrysts, while in "hot" granites the degree of zircon inheritance is much lower (Miller et al., 2003). Hence, the geochemical fingerprint of the Kabalebo charnockites appears to have been produced through melting of a fertile but dehydrated granulitic source under high-temperature conditions.

The Bakhuis granulites present a likely source for the charnockites as the two suites are spatially associated within the BGB. Several lines of reasoning support this assertion. First, resorbed, restitic xenoliths of mafic granulite are locally abundant in the charnockites. These restitic xenoliths are petrographically identical to the mafic granulites of the BGB. Second, the granulites have the required mobile element depleted fingerprint. Absolute alkali- and U–Th-concentrations are over an order of magnitude lower in the granulites compared to the charnockites but their relative depletion is similar (Fig. 6). It is likely that the dehydration and mobile element depletion of the granulites occurred during the UHT metamorphic event at 2.07–2.05 Ga. Subsequent melting of the anhydrous but fertile granulites at 1.98–1.99 Ga produced the Kabalebo charnockites. Third, initial Sr–Nd isotope composition of the granulites and charnockites overlap and thus support a genetic link between the two (Fig. 7). The main difference between the two suites, however, is their contrasting K_2O-content: ~1 wt.% for the intermediate granulites versus 3–5 wt.% for the charnockites. This is, however, a common feature of granulite terrains and associated granitoids, and is likely the result of high-temperature melting of the granulites under anhydrous conditions greatly favouring the release of potassium into the melt (Ebadi and Johannes, 1991).

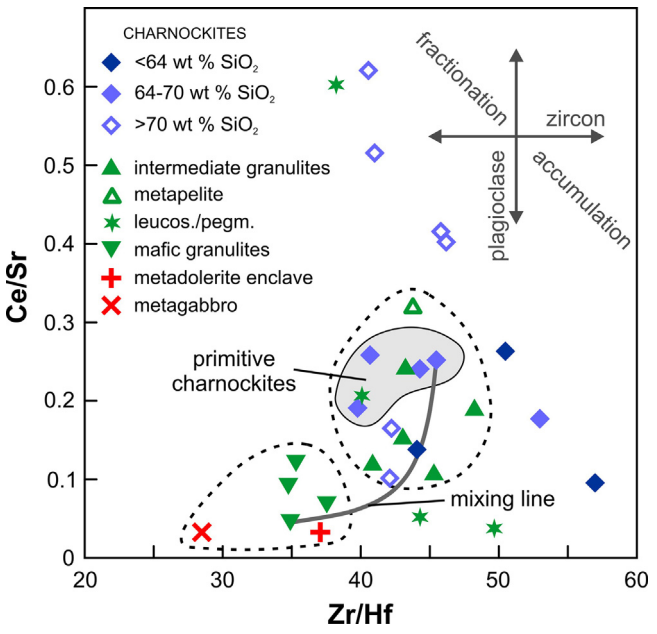

Fig. 9. Ce/Sr vs. Zr/Hf variation plot for the Bakhuis sample suite. The Ce/Sr and Zr/Hf ratios of primitive charnockites with SiO_2 content between 64 and 70 wt.% are identical to the intermediate granulites, but strikingly distinct from the mafic granulites, metagabbro and metadolerite enclave. The large variation in these ratios for other charnockite samples is explained by fractionation and accumulation of plagioclase and zircon. One intermediate charnockite falls on a bulk mixing curve between primitive charnockite (MKS 29) and mafic granulite (MKS 44), suggesting that assimilation of mafic granulite is capable of explaining part of the <64 wt.% charnockites.

To validate if there is a genetic relationship between the Bakhuis granulites and Kabalebo charnockites, we use trace elements ratios of elements with similar incompatibility during melting. A major caveat is that refractory minor phases can retain trace elements during infracrustal melting, thereby severely limiting this application. For the Kabalebo charnockites, we argue that the unusual high-temperature melting conditions have enabled near to complete dissolution of refractory phases such as zircon and apatite so that ratios of these elements in the charnockites should be identical to the protolith. In addition, charnockite REE-patterns do not indicate trace element-rich residual phases such as garnet or amphibole. Pegmatitic veins and leucosomes (>70 wt.% SiO_2) included in the granulite suite do show evidence for residual amphibole as these samples have low trace element concentrations and trough-shaped REE-patterns (Fig. 6) and are hence highly distinct from the BGB charnockites. Fig. 9 shows a Ce/Sr vs. Zr/Hf variation diagram for the Bakhuis samples. Despite the spread in both ratios shown by the charnockites samples, charnockites with SiO_2 content between 64 and 70 wt.% are homogeneous with Ce/Sr = 0.20–0.25 and Zr/Hf = 40–45. As discussed further in Section 6.2.1, we argue that these samples represent the most primitive charnockites within the suite. Their Ce/Sr and Zr/Hf ratios are

identical to the range defined by most intermediate granulites, but are strikingly different from the mafic lithologies. Therefore, we argue that the charnockites are partial melts of the intermediate granulites that constitute about 55% of the Bakhuis Granulite Belt. The presence of restitic mafic granulite xenoliths within the charnockites corroborates melting of the intermediate granulites. The large spread in charnockite Ce/Sr and Zr/Hf ratios is caused by fractional crystallisation and accumulation of plagioclase and/or zircon: fractional crystallisation of plagioclase will increase the Ce/Sr ratio at constant Zr/Hf, zircon fractionation will lead to a decrease in Zr/Hf at near constant Ce/Sr. Accumulation of these phases will have the opposite effect. Both the Ce/Sr and Zr/Hf ratios correlate well with SiO_2-content and petrography. Hence, the displacement of charnockite samples away from the primary charnockite-field in Fig. 9 is explained by plagioclase–zircon fractionation and accumulation.

6.2. Petrogenesis of the Kabalebo charnockites

6.2.1. The parental charnockite and intermediate charnockites

The Kabalebo charnockites form a continuous suite from 64 to 75 wt.% SiO_2 with four intermediate charnockites at 56–61 wt.%. Several lines of evidence suggest that the charnockites at 64–68 wt.% SiO_2 are the most primitive samples, and not the intermediate charnockites. First, we argue that the Kabalebo charnockites are partial melts of the intermediate granulites in the BGB. It appears unlikely that a melt with 56 wt.% SiO_2 could be generated through partial melting of intermediate granulites (55–65 wt.% SiO_2), but 64 wt.% SiO_2 charnockites is possible at high degrees of melting. Second, in the Ce/Sr vs. Zr/Hf diagram (Fig. 9), two of the intermediate charnockites plot at the extreme end of the zircon + plagioclase accumulation trend, while another plots at lower Ce/Sr on a mixing line of primary charnockite with mafic granulite. In contrast, the charnockite samples that are closest to the intermediate granulite field and show no petrographic and geochemical evidence for crystal fractionation or accumulation, are 64–68 wt.% SiO_2 charnockites.

Fig. 10 shows that the four intermediate charnockite samples fall into two distinct groups: a high-Zr/low-Cr and a low-Zr/high-Cr group. Accumulation of fractionating plagioclase and zircon, as suggested by the Ce/Sr and Zr/Hf trends in Fig. 9, will lower the Cr-content while Zr and Sr are strongly enriched. Therefore, the high-Zr/low-Cr intermediate charnockites are best explained through crystal accumulation. In contrast, the low-Zr/high-Cr charnockites do not plot on crystal accumulation trends, but on a mixing line between the parental charnockitic melt and mafic granulites. This suggests that the two low-Zr/high-Cr outliers are the result of local assimilation of mafic granulite. Firm support for this interpretation is provided by field evidence: these two samples occur in areas with a high abundance of restitic, foliated mafic xenoliths (10–20%). Petrographically, these xenoliths match the mafic granulites sampled at Blanche Marie Falls and their resorbed boundaries indicate interaction with the charnockitic melt (Fig. 2). As a result, we argue that the most primitive charnockites are those with 64–68 wt.% SiO_2 while the intermediate charnockites are more evolved, either as cumulates or through assimilation of mafic granulite.

6.2.2. Magmatic differentiation of the charnockite suite

The brick-like texture of plagioclase crystals in some samples suggests enrichment through crystal accumulation. Geochemical evidence for fractionation of predominantly plagioclase over alkali-feldspar is provided by increasing K_2O and Ba/Sr with silica-content (Fig. 6). Fractional crystallisation and removal of plagioclase is supported by decreasing Sr-content in the charnockite suite. There is, however, no correlation between Eu/Eu* and SiO_2 suggesting that REE-rich phases with a negative Eu-anomaly were co-precipitating with plagioclase. On the basis of petrography, zircon and apatite appear to have been fractionating REE-rich phases as they are common in the Kabalebo charnockites. They are relatively enriched in the high-Zr/low-Cr intermediate charnockites and occur predominantly as inclusions in plagioclase instead of interstitially. Decreasing P_2O_5, Zr and REE concentrations and decreasing Zr/Hf with silica-content are in good agreement with early crystallisation of apatite and zircon. These two accessory minerals therefore appear to exert the dominant control on the REE budget of the charnockite suite. Decreasing TiO_2 and Nb with silica-content and relative enrichment of opaque phases in less felsic charnockites is indicative of fractionation of Fe-Ti-oxides. There is a positive correlation between silica-content and hornblende

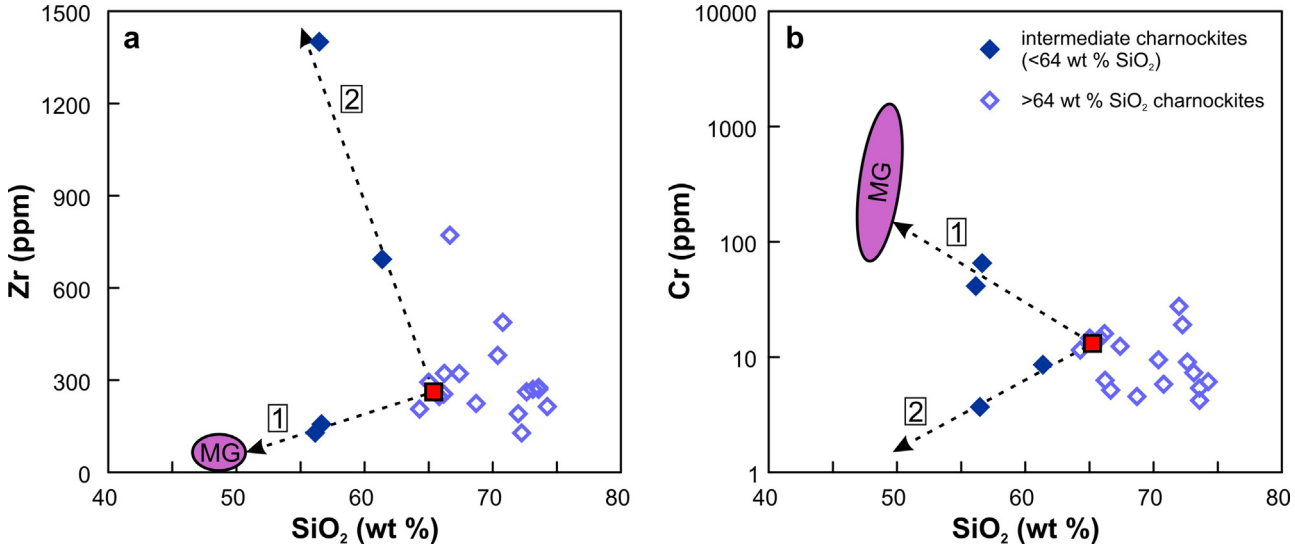

Fig. 10. Trace element variation diagrams depicting the two processes capable of explaining the composition of four intermediate charnockites: [1] mixing of the parental charnockitic melt with mafic granulites through assimilation; and [2] accumulation of plagioclase and zircon through fractional crystallisation. See text for further discussion. Open diamonds: charnockite; red square: hypothetical parental charnockitic melt; grey field "MG": composition of the mafic granulites. Note that true binary mixing curves in the Cr-plot are curved due to the log-scale. (For interpretation of the references to colour in this figure legend, the reader is referred to the web version of this article.)

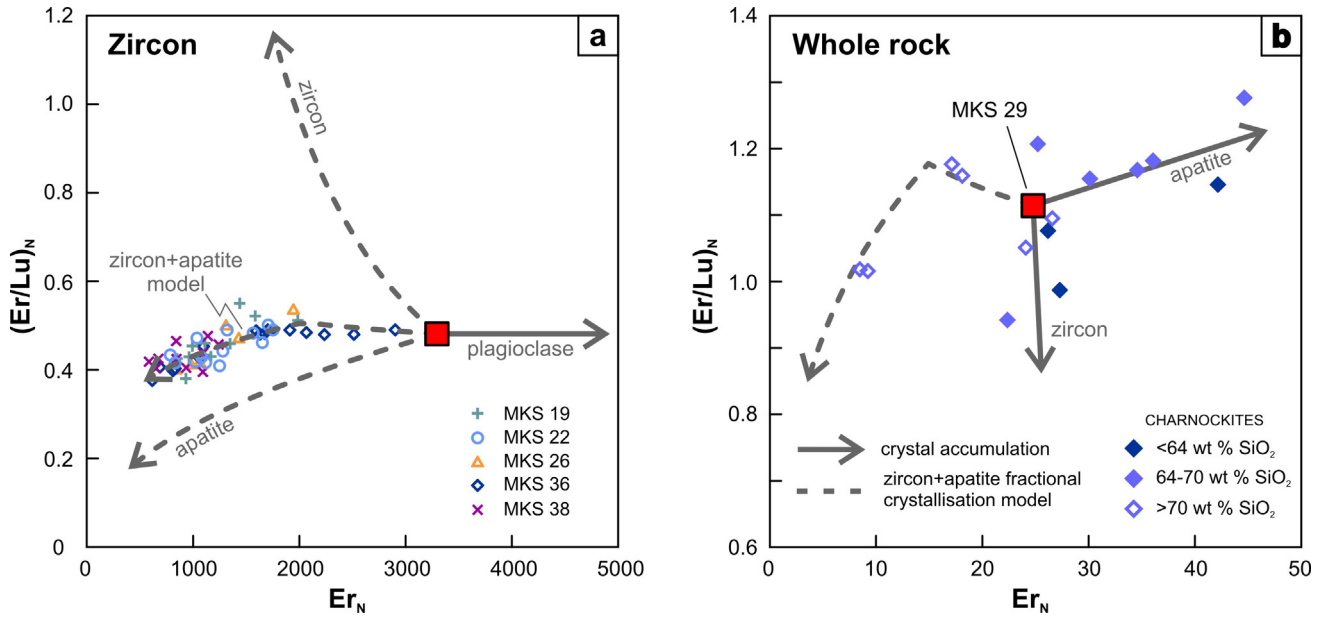

Fig. 11. Results of zircon REE modelling plotted as HREE slope $(Er/Lu)_N$ versus HREE concentration Er_N. See text for further explanation. Subscript "*N*" denotes chrondrite normalised concentrations (McDonough and Sun, 1995); (a) zircon HREE composition combined with modelling results. All samples fall on the combined zircon–apatite fractionation curve, indicating that zircon fractionation alone is not capable of producing the observed zircon HREE variation; (b) whole rock HREE composition plotted against the curve for residual melt composition obtained by the combined zircon–apatite fractionation model. Accumulation of apatite and zircon will lead to increased Er_N at constant $(Er/Lu)_N$. Increased preferential accumulation of zircon will decrease whole rock $(Er/Lu)_N$.

occurrence, hence water appears to have been largely incompatible during fractional crystallisation. This conclusion is corroborated by the fact that hydrous phases and in particular hornblende occur as anhedral, interstitial grains rather than idiomorphic crystals.

Rare-earth element concentrations in zircon from the Kabalebo charnockites vary by more than an order of magnitude. In order to evaluate whether the large REE-variation can be explained by fractionation of zircon and apatite, a fractional crystallisation model is evaluated. Zircon and whole rock rare-earth element concentrations are modelled by incremental Rayleigh fractionation using lattice-strain model (Blundy and Wood, 1994) optimised partition coefficients from Bachmann et al. (2005) for plagioclase and Sano et al. (2002) for zircon and apatite. The latter are selected because they were obtained on co-genetic apatite and zircon and offer the best results when applied to natural samples (Hanchar and van Westrenen, 2007). Charnockite sample MKS 29 is used as the starting composition for the modelling as this sample represents the best approximation of the primary charnockitic melt based on whole rock SiO_2, Zr and REE content and Zr/Hf ratio (see Section 6.2.1). Modelling results are depicted in Fig. 11 where zircon and whole rock heavy rare-earth element slope $(Er/Lu)_N$ and concentration (Er_N) are plotted. Zircon precipitation alone fails to reproduce zircon REE patterns; $(Er/Lu)_N$ increases rapidly to values above unity (i.e. a negative zircon HREE slope). Fractionation of apatite in combination with <0.01% of zircon reproduces the observed decrease in zircon Er_N well, but underestimates the HREE slope by a factor of two. Hence, a combined fractionation of these two phases appears to be required. Zircon HREE variation can satisfactorily be explained by co-precipitation of zircon and apatite in a two-stage model: a first stage of 0.7 wt.% fractionation of apatite and zircon in a 5:1 ratio followed by 2.2 wt.% fractionation of these phases in a 15:1 ratio.

The results of this model are in good agreement with whole rock HREE concentrations as multiple samples plot along the modelled melt-evolution trend. Accumulation of fractionating apatite and zircon is successful in explaining several samples with higher Er_N values compared to "primitive" compositions. P_2O_5-content is positively correlated with Er_N (not shown), which is in line with apatite fractionation as a major control on the REE budget. A negative correlation between silica-content and Er_N further supports that simultaneous fractionation of apatite and zircon exerts the dominant control on the REE budget of the Kabalebo charnockite suite. Hence, the model results demonstrate that whole rock and zircon HREE variation can be explained by simultaneous fractionation of apatite and zircon. Therefore, zircon trace elements support a model with fractional crystallisation as the dominant mechanism responsible for the observed geochemical variation in the charnockite suite and do not provide evidence for significant magma-mixing or crustal assimilation.

6.2.3. *Role of mixing and assimilation*

We have demonstrated that the Kabalebo charnockites are the product of melting of the intermediate granulites in the BGB and that they have differentiated predominantly by fractional crystallisation of plagioclase, zircon and apatite. Nevertheless, field and geochemical evidence points to at least localised interaction with mafic lithologies through assimilation or mixing. The high compatible element content of the low-Zr/high-Cr intermediate charnockites indicates local assimilation of mafic granulite restites (Figs. 2 and 10), and the occurrence of rounded to angular metadolerite enclaves with a quenched ophitic texture in the charnockites suggests the coexistence of a mafic melt that has mingled with the charnockite. These metadolerite enclaves might be related to the larger metagabbro bodies that are present in the southwest of the BGB and represent a possible heat source for charnockite melting. To what degree mixing with a mafic melt has affected the Kabalebo charnockites, is difficult to quantify. Apart from the low-Zr/high-Cr intermediate charnockites, trace element systematics appear to be dominated by fractional crystallisation of accessory phases and mixing or assimilation processes cannot be resolved. The whole rock Sr–Nd isotope composition of the charnockites overlaps with the intermediate granulites, but the metagabbro and metadolerite

have only slightly higher initial $^{143}Nd/^{144}Nd$ (Fig. 7) and their contribution might be masked by the isotopically young composition of the BGB granulites. Zircon hafnium isotope composition supports the whole rock evidence for fractional crystallisation as the dominant mechanism responsible for the geochemical variation in the charnockite suite. The small range in initial zircon ε_{Hf} composition for the five samples is in contrast with granite batholiths where magma-mixing is an influential process (e.g. Hawkesworth and Kemp, 2006). The charnockite samples for which zircon was analysed cover the entire range in silica content observed for the Kabalebo charnockite suite. Mixing of different magma sources should be reflected in a spread in zircon ε_{Hf} that correlates with SiO_2 content. Lack of systematic variation in hafnium isotope composition between samples suggests that mixing of variable magma sources or a significant role for crustal assimilation can be excluded as the major processes responsible for the compositional heterogeneity of the charnockite suite. The absence of core-to-rim Hf isotopic variation in zircon provides further support for this conclusion. Hence, although the occurrence of metadolerite enclaves clearly indicates mingling of the charnockitic melt with a mafic magma, trace element and isotope evidence does not suggest extensive mixing between the two melts.

6.3. The Kabalebo charnockites, UHT metamorphism and the Guiana Shield

6.3.1. Protolith of the BGB granulites

De Roever et al. (2003) interpreted the BGB granulites as a suite of metasedimentary and/or metavolcanic supracrustal rocks with Nd model ages ranging from 2.19 to 2.40 Ga. Hence, these authors suggested that the metasediments were not derived from Archaean crust within or outside the Guiana Shield but suggested a major pulse of crustal accretion during the Transamazonian Orogeny. Our new Nd data yield similar Paleoproterozoic model ages of 2.22–2.34 Ga for the BGB charnockites while the granulites range up to 2.50 Ga. In addition, zircon Hf model ages of the charnockites range from 2.10 to 2.44 Ga with an average of 2.34 Ga and agree well with whole rock Nd model ages. U–Pb dating of sillimanite-gneiss MKS 40 revealed the presence of a population of inherited zircon in this sample (see Section 5.1.2). Zircons in this population are characterised by a magmatically zoned, resorbed core with a metamorphic rim. The magmatically zoned cores yield an age spectrum of ~2.12–2.15 Ga, which is similar to the 2132 and 2153 Ma ages of two inherited grains found by De Roever et al. (2003) in an enderbitic gneiss. These inherited zircon ages overlap with the 2.12–2.18 Ga age of the Guiana TTG-greenstone belt to the east and west of the BGB (Delor et al., 2003a). Major-, trace element and isotope characteristics of the granulites support reworking of a young source with arc-affinity. On the basis of the isotopically young signature and inherited zircon ages, we propose that the protolith of the BGB granulites is detritus derived from the Guiana TTG-greenstone belt without the significant involvement of pre-Transamazonian (>2.25 Ga) crust. Therefore, we concur with De Roever et al. (2003) and Delor et al. (2003a) that the Transamazonian Orogeny constituted a major phase of crustal growth. Nevertheless, there is evidence for limited reworking of Archaean crust in the North Guiana TTG-greenstone belt. Delor et al. (2003b) report negative $\varepsilon_{Nd}(t)$ values up to −10 for intercalated pelites from the northern and southern branch of the greenstone belt in French Guiana, compared to $\varepsilon_{Nd}(t)$ around 0 for the coarser sediments. In contrast, metapelites from the BGB (e.g. MKS 40) do not show highly negative $\varepsilon_{Nd}(t)$ values. Recent zircon dating of CSID-belt volcanic rocks and the Cauarane-Coeroeni belt revealed the presence of a small (~2% of the grains analysed) pre-Transamazonian detrital zircon population (De Roever et al., 2010; Nadeau et al., 2013). The oldest detrital grain encountered yielded a concordant Hadean age of 4219 Ma. This and slightly younger Eoarchaean detrital zircon ages far predate the <3.3 Ga (detrital) zircon ages of the Amapa complex in the eastern part Guiana Shield (Avelar et al., 2003; da Rosa-Costa et al., 2006) and might be derived from the "hidden" Archaean crust to the south of the North Guiana TTG-greenstone belt. In combination with on average older Nd model ages (2.43–2.44 Ga) in CSID volcanic rocks (De Roever et al., 2010), this points to the involvement of Archaean crust in the formation of the rocks from the CSID- and CCB-belts rather than purely reprocessing of Transamazonian crust, as is also suggested by Kroonenberg and de Roever (2010). Therefore, the Kabalebo charnockites and CSID-belt volcanic rocks are most likely derived from distinct sources despite being closely associated in space and time (see Section 6.3.3).

6.3.2. Time gap between charnockite emplacement and UHT metamorphism

The 2072.6 ± 7.3 Ma age for the migmatisation of a sillimanite-gneiss under UHT conditions confirms previous 2055–2072 Ma zircon lead-evaporation ages for the UHT metamorphic event in the BGB (De Roever et al., 2003). In contrast, the Kabalebo charnockites define a narrow range between 1985 and 1993 Ma, at least 60 Myr younger than the UHT metamorphic event. This is in sharp contrast with other UHT terrains where charnockites typically predate or are coeval with peak metamorphic conditions (e.g. Bose et al., 2011; Korhonen et al., 2013; Peng et al., 2012; Rajesh et al., 2014; Zhang et al., 2010). An important implication of this age dichotomy is that two periods with temperatures in excess of 950 °C in the lower crust occurred in the BGB within a time span of 60–90 Myr. The first event at 2.07–2.05 Ga gave rise to the UHT metamorphism, while the second event at 1.99 Ga caused melting of the UHT granulites to form the Kabalebo charnockites. We argue that it is not possible to maintain a thermal anomaly >200 °C in excess of a normal geothermal gradient for such a prolonged period of time. Hence, the BGB must have experienced two separate events in which UHT conditions were achieved. This conclusion raises a myriad of questions about the geodynamic setting of UHT metamorphism and charnockite magmatism, the heat sources required to raise crustal temperatures to >950 °C, the evolution of the Guiana Shield after the main Transamazonian phase, etc., some of which we will address below.

6.3.3. Correlation of the Kabalebo charnockites with other Guiana Shield events

The 1.99 Ga age for charnockite magmatism is clearly distinct from the age of UHT metamorphism in the BGB, but nevertheless there is also evidence for a ~1.98 Ga event in the metamorphic suite. First, zircon from sillimanite-gneiss MKS 40-A (see Section 5.1.2), dating the UHT event at 2073 Ma, is characterised by the typical presence of thin rims around slightly resorbed cores that were too thin for dating by LA-ICPMS. These rims could represent a phase of growth during the 1.98–1.99 Ga thermomagmatic event. In addition, a pegmatite vein sample from De Roever et al. (2003), sampled ~60 km to the NE from the Kabalebo charnockites, yielded three distinct age populations at 2085–2071 Ma, 2059 ± 3 Ma and 1981 ± 3 Ma. De Roever et al. (2003) interpreted 2059 Ma as the age of pegmatite vein crystallisation and the younger age as overprint from a younger event. Overprint of this pegmatite during charnockite emplacement is possible, but raises the question why none of the other granulite samples from the same locality show evidence for recrystallization. Another possibility is that the 1981 Ma age dates pegmatite crystallisation related to charnockite magmatism, with the older ages representing inherited zircons.

Charnockite magmatism at 1.99 Ga is coeval with widespread felsic volcanism and subvolcanic granitoid intrusions that form the CSID-belt, which ranges from western Suriname and Guyana

to Brazil and Venezuela (Fig. 1). A felsic metavolcanic rock and a leucogranite from western Suriname have been dated at 1987 ± 4 and 1980 ± 4 Ma respectively (De Roever et al., 2010), which represent the first precise age determinations for the CSID-belt (locally known as the Dalbana formation) in western Suriname. In addition, their equivalents in Guyana (Iwokrama formation) were dated at 1980–1991 Ma (Nadeau et al., 2013) and these results agree well with the 1.98 Ga ages for the Surumu volcanic rocks from Brazil (Reis et al., 2000; Santos et al., 2003). This suggests that the Kabalebo charnockites might be related to the 1.99–1.98 Ga CSID-belt of felsic volcanism that surrounds the BGB, even though they appear to be derived from distinct sources on the basis of inherited zircon ages. Further geochemical research is required to establish a connection between the two. The timing of granulite-facies metamorphism in the Cauarane-Coeroeni Belt to the south of the BGB and CSID-belt has recently been constrained at 2.01–1.98 (De Roever et al., 2010; Fraga et al., 2009), which is roughly contemporaneous with emplacement of the Kabalebo charnockites and felsic volcanism. Hence, there is growing evidence that the collision between the West African and Amazonian Cratons was not completed at the end of the main Transamazonian phase (~2.06 Ga). Although this event marks the suturing of the TTG-greenstone belt with the Archaean Amapa block and the West African Shield in French Guiana and Brazil, the 2.00–1.98 magmatism and metamorphism further to the west suggest the formation of a new active continental margin at the southern side of the TTG-greenstone belt, with subduction and convergence to the north (Fraga et al., 2009). The final stabilisation of a combined Amazonian-West African Shield is constrained by the deposition of the unfolded Roraima sandstones (see Fig. 1) at 1.87 Ga (Santos et al., 2003) or even as early as 1.90 Ga (Minter, 2006).

6.3.4. Heat sources for UHT metamorphism and charnockite magmatism

UHT metamorphism and anhydrous melting at temperatures in excess of 950 °C as observed in the BGB cannot be achieved in a normal collisional setting without invoking high concentrations of heat producing elements and crustal thickening (e.g. Clark et al., 2011; Collins, 2002). This scenario is not viable for the UHT metamorphism in the BGB for two reasons: (i) the BGB granulites are strongly depleted in U-Th-K, and (ii) the granulites record near-isobaric heating and cooling (De Roever et al., 2003). Hence, an external heat source is required to explain the two >950 °C events in the BGB. The involvement of advective mantle heat sources and primitive mantle melts in the genesis of charnockites and UHT metamorphism has been acknowledged in multiple studies (e.g. Liu et al., 2006; Peng et al., 2012; Santosh et al., 2012; Zhang et al., 2010). In particular, Peng et al. (2010, 2012) report the contribution of up to 60% of juvenile gabbronorite related to ridge subduction. Many (meta)gabbroic bodies are present in the BGB and these appear to be concentrated in the southwest (Fig. 1). It is not clear whether these mafic intrusions represent a single event or constitute multiple generations, but the variable degree of metamorphic overprint points towards more than one generation with older metagabbros and younger, non-recrystallized gabbros. The lack of foliation in the metagabbros indicates that they postdate the main phase of UHT metamorphism with synchronous folding, while the presence of metadolerite enclaves within the charnockites suggests that the metagabbros are likely synchronous with the charnockite magmatism at 1.99 Ga. This conclusion is supported by the 1980 ± 5 Ma age for a layered anorthosite body in the core of the BGB that is potentially related to the metagabbros (De Roever et al., 2003). Although two metadolerite dikes within the BGB granulites were dated at 2056 ± 4 and 2060 ± 4 Ma by the zircon Pb–Pb evaporation method (De Roever et al., 2003), re-examination of zircon from these samples indicates that it is most likely xenocrystic and the 2056–2060 Ma ages probably do not date the intrusion of the dikes. Hence, these lines of evidence suggest that mafic magmatism in the BGB postdates the main UHT and deformation event and is synchronous with charnockite emplacement. High-precision dating of the (meta)gabbros is, however, required to confirm this hypothesis. We propose that the intrusion of voluminous hot, mafic magma into the lower crust, which probably retained some excess heat from the UHT event ~60 Myr previously, was the direct cause of local melting of the granulite suite to produce the charnockites. The presence of primary amphibole and negative Nb–Ta anomaly in the metagabbro point towards an origin in a subduction zone environment. This conclusion is in line with the evidence for the development of an active continental margin at the southern side of the TTG-greenstone belt complex during the late Transamazonian phase outlined in Section 6.3.3.

The new geochronological evidence suggests that the UHT metamorphism was not accompanied by large-scale mafic or felsic magmatism within the BGB or the nearby parts of the Guiana Shield, with the exception of localised monzogranite intrusions related to shearing in French Guiana (around 2065 Ma (Delor et al., 2003a). This is not anomalous as numerous UHT localities are characterised by an absence of voluminous contemporaneous mafic magmatism (Kelsey and Hand, 2014 and references therein). In addition, UHT metamorphism postdates the suturing of the North Guiana TTG-greenstone belt and the West African Shield at 2.11–2.08 Ga by at least 10 Myr and hence could be the result of post-collisional slab break-off (Harley, 2008). Alternatively, UHT metamorphism in the BGB could be the result of thickening of a back-arc basin south of the TTG-greenstone belt, which is a popular model to account for the occurrence of UHT conditions (e.g. Brown, 2006; Clark et al., 2011; Collins, 2002; Kelsey and Hand, 2014). A change from an extensional to a compressional regime south of the TTG-greenstone belt after suturing with the West African Shield agrees well with our inference of a change in subduction direction and the development of an active continental margin during the late Transamazonian phase, but has two major issues. First, a back-arc regime is a notoriously wet environment, which is at odds with the dehydrated nature of most UHT terrains (including the BGB) and the need for a low water activity to suppress melting (Kelsey and Hand, 2014; Santosh and Kusky, 2010). Second, the UHT granulites in the BGB comprise predominantly metasediments derived from the TTG-greenstone belt. We find it hard to envisage how detritus from the TTG-greenstone belt can be transported to a depth of around 30 km (0.85–0.90 GPa; De Roever et al., 2003) through a back-arc setting. In contrast, subcretion of fore-arc sediments during southward subduction (2.18–2.12 Ga) is a plausible mechanism to place the metasediments at the base of the TTG-greenstone complex. This raises the question whether the 2.07–2.05 Ga UHT metamorphism is restricted to the BGB or if it is a regional feature of the north Guiana TTG-greenstone belt that is only exposed in the BGB. Granulite-facies metamorphism did occur roughly contemporaneously with the BGB event in the Amapa (2.09–2.08 Ga; (da Rosa-Costa et al., 2008) and Imataca (2.05–1.98 Ga; (Tassinari et al., 2004) complexes, but was considerably lower grade. Hence, we prefer an explanation in which the special position of the BGB favoured the occurrence of UHT conditions. We postulate that the collision with the Amapa block stabilised the eastern part of the Shield by 2.08 Ga while convergence continued in the west, leading to crustal-scale sinistral shearing and boudinage as proposed by Delor et al. (2003a). As a consequence of this extension, a slab tear developed in the subducted West African slab at the boundary between the two domains, resulting in localised asthenosperic upwelling. The BGB, situated at this boundary, received a large input of heat that led to UHT metamorphism and a CO_2 flux sufficient to supress dehydration melting (Santosh and Omori, 2008). It remains enigmatic, however, how such a process would leave no traces in

the form of mafic magmatism and clearly this invites further studies into the origin of UHT metamorphism in the BGB.

6.3.5. A single, long-lived UHT event?

The arguments presented above are based on our assumption that it is impossible to maintain a temperature >950 °C in the lower crust for 60–90 Myr. Recent studies, however, do suggest that UHT conditions can be extremely long-lived, based on >100 Myr spreads in monazite and to a lesser extent zircon U/Pb spot ages in (U)HT rocks of the Eastern Ghats Belt, India (e.g. Korhonen et al., 2013) and the Proterozoic Musgrave and Arunta terrains in Australia (Morrissey et al., 2014; Walsh et al., 2014). In these studies, peak metamorphic conditions are fairly well constrained in time and the monazite spot ages are both older, indicative of prograde growth, and up to 70 Myr younger, which suggests continuous monazite growth during very slow cooling at rates of 0.5–1.5 °C/Myr (Walsh et al., 2014). These timespans are remarkably similar to the 60–90 Myr gap between UHT metamorphism and charnockite magmatism in the BGB. Moreover, cooling from 1025 °C at 2073 Ma (sillimanite-gneiss MKS 40) to 960 °C at 1985 Ma (Kabalebo charnockites) is in agreement with a cooling rate of 0.6–0.8 °C/Myr, again similar to these long-lived UHT events. This raises the question if our assumption of two discrete UHT events in the BGB is justified or whether the Guiana Shield comprises another example of Precambrian long-lived UHT conditions.

There are some marked differences between the BGB and the Indian-Australian UHT events. Primarily, the proposed continuum of ages is not found in the BGB. No ages between 2055 and 1993 Ma have so far been documented in the BGB and all available ages cluster at either 2.07–2.05 Ga or 1.99–1.98 Ga, although this might be due to undersampling. Interestingly, De Roever et al. (2003) report weighted average monazite ages analysed by electron-microprobe for three granulite samples that range from 2127 ± 15 to 2007 ± 11 Ma and hence pre- and postdate the UHT event. The significance of these ages, however, is uncertain and further monazite U/Pb studies could provide valuable information. Another major difference is the timing of associated magmatism. Whereas in the Eastern Ghats Belt granitic and charnockite magmatism is roughly contemporaneous with peak PT conditions (Bose et al., 2011; Korhonen et al., 2013), the Kabalebo charnockites postdate the UHT event by at least 60 Myr. This raises the important question of why the granulites would suddenly melt to form a charnockitic melt during slow cooling. In theory, mafic underplating could release a hydrous fluid phase that lowers the solidus of the overlying granulites, causing wet melting, without a significant increase in temperature. This scenario, however, disagrees with the anhydrous nature of the Kabalebo charnockites. A much more simple explanation is the model proposed in Section 6.3.4: the emplacement of the hot metagabbroic melt raises the temperature sufficiently to induce melting of the dehydrated granulites. Although we argue that the BGB still retained some of the UHT heat that favoured melting at 1.99 Ga, this scenario eliminates the need for very slow cooling. It remains enigmatic how UHT conditions can be maintained over timescales in excess of 100 Myr. Smithies et al. (2011) evoke the presence of a lower crustal melting-assimilation-storage-homogenization (MASH) zone over the lifetime of the UHT conditions in the Australian Musgrave terrain, which is supported by a continuous spectrum in coeval granitoid ages. Due to the absence of any 2.05–2.00 Ga ages in the BGB, we favour the simpler explanation of two separate UHT events in the BGB.

7. Conclusions

The Kabalebo charnockites represent a coherent suite of orthopyroxene-bearing granitoids within the ultrahigh-temperature Bakhuis Granulite Belt. Ternary feldspar and inverted pigeonite indicate crystallisation temperatures between 960 and 990 °C and the geochemical characteristics of the charnockites attest to derivation from a dehydrated but fertile granulite source. Field, trace element and Sr–Nd isotope evidence indicate that the Kabalebo charnockites are the product of partial melting of the UHT granulite suite, but charnockite magmatism postdates UHT metamorphism by at least 60 Myr. New U–Pb zircon ages of five charnockite samples are identical within error and range from 1984.4 to 1992.5 Ma, while zircon from a leucosome formed under UHT conditions yielded 2172.6 ± 7.3 Ma. The important implication of this age difference is that two periods with temperatures in excess of 950 °C occurred in the lower crust within a time span of 60–90 Myr. Field evidence suggests that (meta)gabbroic intrusions are contemporaneous with and the likely heat source for charnockite magmatism. In contrast, the UHT metamorphic event appears not to be associated with significant mafic magmatism and crustal melting in the BGB or nearby Guiana Shield and its origin remains uncertain. In the light of the new geochemical and geochronological data, we propose that the Paleoproterozoic collision between the Amazonian and West African Shields continued after the end of the main Transamazonian phase (2.06 Ga). Suturing of the north Guiana TTG-greenstone belt with West Africa and the Amapa block at 2.11–2.08 Ga stabilised the eastern domain of the Guiana Shield. A change in subduction direction and consequential sinistral shearing possibly caused the opening of a slab window, mantle upwelling and UHT metamorphism in the Bakhuis Granulite Belt. Initiation of northward subduction in the western domain led to the formation of a large belt of felsic volcanic rocks and subvolcanic granites, with which the Kabalebo charnockites are at least spatially and temporally associated. Important developments have been made in the recent years towards the understanding of the evolution of the Guiana Shield, but clearly more geochronological and geochemical research into the late Transamazonian phase is required. In addition, the origin of UHT metamorphism in the BGB is not well understood and requires further investigation of how the lower crust can be heated to >1000 °C without the involvement of mafic magmatism and associated crustal melting.

Acknowledgements

We would like to thank the staff at Kabalebo Nature Resort and in particular Karel and Joyce Dawson for their support of the field campaign in the jungle of Suriname. The Geological and Mining Service of Suriname and Mr. Autar are thanked for their assistance. The technical staff at VU University and Utrecht University provided invaluable help in the labs and in particular Suzette Timmerman is greatly acknowledged for doing part of the EMP analyses. Wim van Westrenen is thanked for his helpful advice on the zircon trace element modelling and Jan Wijbrans for his help with the interpretation of the U/Pb data. The manuscript greatly benefited from the constructive reviews of H.M. Rajesh and J. Touret, and the comments by B.R. Frost on a previous version. Randall Parrish is thanked for careful editorial handling. Financial support was provided by the Dr. Schürmann Foundation (grant number 53/2008) and Stichting Molengraaff Funds (grant number 2009-01).

Appendix A. Supplementary data

Supplementary data associated with this article can be found, in the online version, at http://dx.doi.org/10.1016/j.precamres.2015.02.014.

References

Almeida, M.E., Macambira, M.J.B., Oliveira, E.C., 2007. Geochemistry and zircon geochronology of the I-type high-K calc-alkaline and S-type granitoid rocks from southeastern Roraima Brazil: Orosirian collisional magmatism evidence (1.97–1.96 Ga) in central portion of Guyana Shield. Precambrian Res. 155, 69–97.

Avelar, V.d., Lafon, J., Delor, C., Guerrot, C., Lahondère, D., Rossi, P., Lafon, J., Vasquez, M., 2003. Archean crustal remnants in the easternmost part of the Guiana Shield: Pb–Pb and Sm–Nd geochronological evidence for Mesoarchean versus Neoarchean signatures. Géol. France 2, 3–4.

Bachmann, O., Dungan, M.A., Bussy, F., 2005. Insights into shallow magmatic processes in large silicic magma bodies: the trace element record in the Fish Canyon magma body, Colorado. Contrib. Mineral. Petrol. 149, 338–349.

Bhattacharya, S., 2010. Review: the charnockite problem, a twenty first century perspective. Nat. Sci. 2, 402–408.

Blundy, J., Wood, B., 1994. Prediction of crystal–melt partition coefficients from elastic moduli. Nature 372, 452–454.

Bose, S., Dunkley, D.J., Dasgupta, S., Das, K., Arima, M., 2011. India–Antarctica–Australia–Laurentia connection in the Paleoproterozoic–Mesoproterozoic revisited: evidence from new zircon U–Pb and monazite chemical age data from the Eastern Ghats Belt, India. Geol. Soc. Am. Bull. 123, 2031–2049.

Bouvier, A., Vervoort, J.D., Patchett, P.J., 2008. The Lu–Hf and Sm–Nd isotopic composition of CHUR: constraints from unequilibrated chondrites and implications for the bulk composition of terrestrial planets. Earth Planet. Sci. Lett. 273, 48–57.

Brown, M., 2006. Duality of thermal regimes is the distinctive characteristic of plate tectonics since the Neoarchean. Geology 34, 961–964.

Brown, M., Korhonen, F.J., 2009. Some Remarks on Melting and Extreme Metamorphism of Crustal Rocks Physics and Chemistry of the Earth's Interior. Springer, pp. 67–87.

Claiborne, L.L., Miller, C., Walker, B., Wooden, J., Mazdab, F., Bea, F., 2006. Tracking magmatic processes through Zr/Hf ratios in rocks and Hf and Ti zoning in zircons: an example from the Spirit Mountain batholith, Nevada. Mineral. Mag. 70, 517–543.

Clark, C., Fitzsimons, I.C., Healy, D., Harley, S.L., 2011. How does the continental crust get really hot? Elements 7, 235–240.

Collins, W., 2002. Hot orogens, tectonic switching, and creation of continental crust. Geology 30, 535–538.

Cordani, U.G., Fraga, L.M., Reis, N., Tassinari, C.C., Brito-Neves, B.B., 2010. On the origin and tectonic significance of the intra-plate events of Grenvillian-type age in South America: a discussion. J. S. Am. Earth Sci. 29, 143–159.

da Rosa-Costa, L.T., Lafon, J.M., Delor, C., 2006. Zircon geochronology and Sm–Nd isotopic study: further constraints for the Archean and Paleoproterozoic geodynamical evolution of the southeastern Guiana Shield, north of Amazonian Craton, Brazil. Gondwana Res. 10, 277–300.

da Rosa-Costa, L., Lafon, J., Cocherie, A., Delor, C., 2008. Electron microprobe U–Th–Pb monazite dating of the Transamazonian high-grade metamorphic overprint on Archean rocks from Amapa block, southeastern Guiana Shield, Northern Brazil. J. S. Am. Earth Sci. 26, 445–462.

De Roever, E.W.F., Lafon, J.-M., Delor, C., Cocherie, A., Rossi, P., Guerrrot, C., Potrel, A., 2003. The Bakhuis ultrahigh-temperature granulite belt (Suriname): I. Petrological and geochronological evidence for a counterclockwise P–T path at 2.07–2.05 Ga. Géol. France 2-3-4, 175–205.

De Roever, E.W.F., Lafon, J.-M., Delor, C., Guerrrot, C., 2010. Orosirian magmatism and metamorphism in Surinam: new geochronological constraints. In: 45th Congresso Brasileiro de Geologia, Belem, Brasil.

Delor, C., De Roever, E.W.F., Lafon, J.-M., Lahondère, D., Rossi, P., Cocherie, A., Guerrrot, C., Potrel, A., 2003a. The Bakhuis ultrahigh-temperature granulite belt (Suriname): II. Implications for late Transamazonian crustal stretching in a revised Guiana Shield framework. Géol. France 2-3-4, 207–230.

Delor, C., Lahondère, D., Egal, E., Lafon, J.-M., Cocherie, A., Guerrot, C., Rossi, P., Truffert, C., Théveniaut, H., Phillips, D., De Avelar, V.G., 2003b. Transamazonian crustal growth and reworking as revealed by the 1:500,000-scale geological map of French Guiana (2nd edition). Géol. France 2-3-4, 5–57.

DePaolo, D.J., 1981. Neodymium Isotopes in the Colorado Front Range and Crust–Mantle Evolution in the Proterozoic. Nature 291, 193–196.

Ebadi, A., Johannes, W., 1991. Beginning of melting and composition of first melts in the system Qz–Ab–Or–H_2O–CO_2. Contrib. Mineral. Petrol. 106, 286–295.

Ferry, J.M., Watson, E.B., 2007. New thermodynamic models and revised calibrations for the Ti-in-zircon and Zr-in-rutile thermometers. Contrib. Mineral. Petrol. 154, 429–437.

Fraga, L.M., Reis, N.J., Dall'Agnol, R., 2009. Cauarane-Coeroeni Belt: the main tectonic feature of the Central Guyana Shield Northern Amazonian Craton. In: Simpósio de Geologia da Amazônia, vol. 11, pp. 02–05.

Frost, B.R., Frost, C.D., 2008. On charnockites. Gondwana Res. 13, 30–44.

Frost, B.R., Barnes, C.G., Collins, W.J., Arculus, R.J., Ellis, D.J., Frost, C.D., 2001. A geochemical classification for granitic rocks. J. Petrol. 42, 2033–2048.

Fuhrman, M.L., Lindsley, D.H., 1988. Ternary-feldspar modeling and thermometry. Am. Mineral. 73, 201–215.

Hanchar, J.M., van Westrenen, W., 2007. Rare earth element behavior in zircon-melt systems. Elements 3, 37–42.

Harley, S.L., 2008. Refining the P–T records of UHT crustal metamorphism. J. Metamorph. Geol. 26, 125–154.

Harrison, T.M., Watson, E.B., 1984. The behavior of apatite during crustal anatexis: equilibrium and kinetic considerations. Geochim. Cosmochim. Acta 48, 1467–1477.

Hawkesworth, C.J., Kemp, A.I.S., 2006. Using hafnium and oxygen isotopes in zircons to unravel the record of crustal evolution. Chem. Geol. 226, 144–162.

Hildebrand, R.S., Buchwaldt, R., Bowring, S.A., 2014. On the allochthonous nature of auriferous greenstones, Guayana shield Venezuela. Gondwana Res. 26, 1129–1140.

Hoskin, P.W.O., Schaltegger, U., 2003. The composition of zircon and igneous and metamorphic petrogenesis. Rev. Mineral. Geochem. 53, 27–62.

Kelsey, D.E., Hand, M., 2014. On ultrahigh temperature crustal metamorphism: phase equilibria, trace element thermometry, bulk composition, heat sources, timescales and tectonic settings. Geosci. Front., http://dx.doi.org/10.1016/j.gsf.2014.09.006, in press.

Keppler, H., Wyllie, P.J., 1990. Role of fluids in transport and fractionation of uranium and thorium in magmatic processes. Nature 348, 531–533.

Kilpatrick, J.A., Ellis, D.J., 1992. C-type magmas: igneous charnockites and their extrusive equivalents. Trans. R. Soc. Edinb.: Earth Sci. 83, 155–164.

Korhonen, F., Clark, C., Brown, M., Bhattacharya, S., Taylor, R., 2013. How long-lived is ultrahigh temperature (UHT) metamorphism? Constraints from zircon and monazite geochronology in the Eastern Ghats orogenic belt, India. Precambrian Res. 234, 322–350.

Kroonenberg, S.B., 1976. Amphibolite–facies and granulite–facies metamorphism in the Coeroeni-Lucie area, southwestern Suriname. Geol. Mijnbouwkund. Dienst Suriname Meded. 25, 109–289.

Kroonenberg, S.B., de Roever, E.W., 2010. Geological evolution of the Amazonian Craton. In: Amazonia, Landscape and Species Evolution: A Look into the Past., pp. 7–28.

Linnen, R.L., Keppler, H., 2002. Melt composition control of Zr/Hf fractionation in magmatic processes. Geochim. Cosmochim. Acta 66, 3293–3301.

Liu, X., Jahn, B.-M., Zhao, Y., Li, M., Li, H., Liu, X., 2006. Late Pan-African granitoids from the Grove Mountains East Antarctica: age, origin and tectonic implications. Precambrian Res. 145, 131–154.

McDonough, W.F., Sun, S.S., 1995. The composition of the Earth. Chem. Geol. 120, 223–253.

Miller, C.F., McDowell, S.M., Mapes, R.W., 2003. Hot and cold granites? Implications of zircon saturation temperatures and preservation of inheritance. Geology 31, 529–532.

Minter, W.E.L., 2006. The sedimentary setting of Witwatersrand placer mineral deposits in an Archean atmosphere. Geol. Soc. Am. Mem. 198, 105–119.

Morrissey, L., Hand, M., Raimondo, T., Kelsey, D., 2014. Long-lived high-T, low-P granulite facies metamorphism in the Arunta Region, central Australia. J. Metamorph. Geol. 32, 25–47.

Nadeau, S., Chen, W., Reece, J., Lachhman, D., Ault, R., Faraco, M.T.L., Fraga, L.M., Reis, N.J., Betiollo, L.M., 2013. Guyana: the Lost Hadean crust of South America? Braz. J. Geol. 43, 601–606.

Newton, R.C., 1992. An overview of charnockite. Precambrian Res. 55, 399–405.

Norcross, C., Davis, D.W., Spooner, E.T., Rust, A., 2000. U–Pb and Pb–Pb age constraints on Paleoproterozoic magmatism, deformation and gold mineralization in the Omai area, Guyana Shield. Precambrian Res. 102, 69–86.

Padoan, M., Rossetti, P., Rubatto, D., 2014. The Choco 10 Gold Deposit (El Callao, Bolivar State, Venezuela): petrography geochemistry and U–Pb geochronology. Precambrian Res. 252, 22–38.

Peng, P., Guo, J., Zhai, M., Bleeker, W., 2010. Paleoproterozoic gabbronoritic and granitic magmatism in the northern margin of the North China Craton: evidence of crust–mantle interaction. Precambrian Res. 183, 635–659.

Peng, P., Guo, J., Windley, B., Liu, F., Chu, Z., Zhai, M., 2012. Petrogenesis of Late Paleoproterozoic Liangcheng charnockites and S-type granites in the central-northern margin of the North China Craton: implications for ridge subduction. Precambrian Res. 222, 107–123.

Priem, H.N.A., Boelrijk, N.A.I.M., Hebeda, E.H., Verdurmen, E.A.T., Verschure, R.H., 1971. Isotopic ages of the Trans-Amazonian acidic magmatism and the Nickerie metamorphic episode in the Precambrian basement of Suriname, South America. Geol. Soc. Am. Bull. 82, 1667–1680.

Rajesh, H.M., Santosh, M., 2012. Charnockites and charnockites. Geosci. Front. 3, 737–744.

Rajesh, H., Santosh, M., Wan, Y., Liu, D., Liu, S., Belyanin, G., 2014. Ultrahigh temperature granulites and magnesian charnockites: evidence for Neoarchean accretion along the northern margin of the Kaapvaal Craton. Precambrian Res. 246, 150–159.

Reis, N.J., De Faria, M.S.G., Fraga, L.M., Haddad, R.C., 2000. Orosirian calc-alkaline volcanism and the Orocaima event in the northern Amazonian Craton, eastern Roraima state, Brazil. Rev. Bras. Geocienc. 30, 380–383.

Rudnick, R., Gao, S., 2003. Composition of the continental crust. Treatise Geochem. 3, 1–64.

Rudnick, R., Presper, T., 1990. Geochemistry of intermediate-to high-pressure granulites. In: Granulites and Crustal Evolution., pp. 523–550.

Sano, Y., Terada, K., Fukuoka, T., 2002. High mass resolution ion microprobe analysis of rare earth elements in silicate glass, apatite and zircon: lack of matrix dependency. Chem. Geol. 184, 217–230.

Santos, J.O.S., Potter, P.E., Reis, N.J., Hartmann, L.A., Fletcher, I.R., McNaughton, N.J., 2003. Age, source, and regional stratigraphy of the Roraima Supergroup and Roraima-like outliers in northern South America based on U–Pb geochronology. Geol. Soc. Am. Bull. 115, 331–348.

Santos, J.O.S., Van Breemen, O.B., Groves, D.I., Hartmann, L.A., Almeida, M.E., McNaughton, N.J., Fletcher, I.R., 2004. Timing and evolution of multiple Paleoproterozoic magmatic arcs in the Tapajós Domain Amazon Craton: constraints from SHRIMP and TIMS zircon, baddeleyite and titanite U–Pb geochronology. Precambrian Res. 131, 73–109.

Santosh, M., Kusky, T., 2010. Origin of paired high pressure–ultrahigh-temperature orogens: a ridge subduction and slab window model. Terra Nova 22, 35–42.

Santosh, M., Omori, S., 2008. CO_2 flushing: a plate tectonic perspective. Gondwana Res. 13, 86–102.

Santosh, M., Liu, S., Tsunogae, T., Li, J., 2012. Paleoproterozoic ultrahigh-temperature granulites in the North China Craton: implications for tectonic models on extreme crustal metamorphism. Precambrian Res. 222, 77–106.

Scherer, E., Münker, C., Mezger, K., 2001. Calibration of the Lutetium-Hafnium Clock. Science 293, 683–687.

Smithies, R.H., Howard, H.M., Evins, P.M., Kirkland, C.L., Kelsey, D.E., Hand, M., Wingate, M.T.D., Collins, A.S., Belousova, E., 2011. High-temperature granite magmatism, crust–mantle interaction and the mesoproterozoic intracontinental evolution of the Musgrave Province Central Australia. J. Petrol. 52, 931–958.

Sun, S.S., McDonough, W.F., 1989. Chemical and isotopic systematics of oceanic basalts: implications for mantle composition and processes. Geol. Soc. Lond. Spec. Publ. 42, 313–345.

Tassinari, C.C., Munhá, J.M., Teixeira, W., Palácios, T., Nutman, A.P., Sosa, C., Santos, A.P., Calado, B.O., 2004. The Imataca Complex, NW Amazonian Craton Venezuela: crustal evolution and integration of geochronological and petrological cooling histories. Epis.-Newsmag. Int. Union Geol. Sci. 27, 3–12.

Thorpe, R., Hickman, A., Davis, D., Mortensen, J., Trendall, A., 1992. U–Pb zircon geochronology of Archaean felsic units in the Marble Bar region, Pilbara Craton, Western Australia. Precambrian Res. 56, 169–189.

Touret, J.L.R., Huizenga, J.M., 2012. Charnockite microstructures: from magmatic to metamorphic. Geosci. Front. 3, 745–753.

Valério, C.d.S., Souza, V.d.S., Macambira, M.J.B., 2009. The 1.90–1.88 Ga magmatism in the southernmost Guyana Shield, Amazonas Brazil: geology, geochemistry, zircon geochronology, and tectonic implications. J. S. Am. Earth Sci. 28, 304–320.

Walsh, A., Kelsey, D., Kirkland, C., Hand, M., Smithies, R., Clark, C., Howard, H., 2014. P–T–t evolution of a large, long-lived, ultrahigh-temperature Grenvillian belt in central Australia. Gondwana Res., http://dx.doi.org/10.1016/j.gr.2014.05.012, in press.

Watson, E.B., Harrison, T.M., 1983. Zircon saturation revisited: temperature and composition effects in a variety of crustal magma types. Earth Planet. Sci. Lett. 64, 295–304.

Young, D.N., Zhao, J.-x., Ellis, D.J., McCulloch, M.T., 1997. Geochemical and Sr–Nd isotopic mapping of source provinces for the Mawson charnockites, east Antarctica: implications for Proterozoic tectonics and Gondwana reconstruction. Precambrian Res. 86, 1–19.

Zhang, Z., Zhao, G., Santosh, M., Wang, J., Dong, X., Shen, K., 2010. Late Cretaceous charnockite with adakitic affinities from the Gangdese batholith, southeastern Tibet: evidence for Neo-Tethyan mid-ocean ridge subduction? Gondwana Res. 17, 615–631.

Zhao, J.-x., Ellis, D.J., Kilpatrick, J.A., McCulloch, M.T., 1997. Geochemical and Sr–Nd isotopic study of charnockites and related rocks in the northern Prince Charles Mountains East Antarctica: implications for charnockite petrogenesis and proterozoic crustal evolution. Precambrian Res. 81, 37–66.